

Article

Feasibility Study of a Fan-Driven Device Generating Downforce for Road Cars

Maciej Szudarek ¹, Adam Piechna ² and Janusz Piechna ^{3,*}

¹ Institute of Metrology and Biomedical Engineering, Warsaw University of Technology, 02-525 Warszawa, Poland; maciej.szudarek@pw.edu.pl

² Institute of Automatic Control and Robotics, Warsaw University of Technology, 02-525 Warszawa, Poland; adam.piechna@pw.edu.pl

³ Institute of Aeronautics and Applied Mechanics, Warsaw University of Technology, 00-665 Warszawa, Poland

* Correspondence: janusz.piechna@pw.edu.pl

Abstract: This paper, submitted to the special issue of Energies “Future of Road Vehicle Aerodynamics”, proposes and justifies the use of an old idea of generating downforce by actively drawing air from under the car body and exhausting it to the outside. Instead of traditional moving mechanical-curtain elements, a new method for sealing the clearance under the body with an air curtain is proposed. Basic information on the geometry and flow characteristics of such a solution suitable for use in automobiles is presented. The performance of such a fan-driven device generating downforce is studied over a wide range of driving speeds. The device allows for significantly improved vehicle acceleration, shorter braking distances, and extension of the range of safe cornering speeds. The paper shows the successive stages of development of the idea, from the 2D model to the 3D model, and an attempt to implement the device on a sports car. The distributions of pressure, velocity, pathlines and values of aerodynamic forces obtained at assumed fan compressions for different driving speeds are presented. The advantages and disadvantages of the analyzed device are discussed, and further optimization directions are outlined.



Citation: Szudarek, M.; Piechna, A.; Piechna, J. Feasibility Study of a Fan-Driven Device Generating Downforce for Road Cars. *Energies* **2022**, *15*, 5549. <https://doi.org/10.3390/en15155549>

Academic Editor: Galih Bangga

Received: 28 June 2022

Accepted: 28 July 2022

Published: 30 July 2022

Publisher’s Note: MDPI stays neutral with regard to jurisdictional claims in published maps and institutional affiliations.



Copyright: © 2022 by the authors. Licensee MDPI, Basel, Switzerland. This article is an open access article distributed under the terms and conditions of the Creative Commons Attribution (CC BY) license (<https://creativecommons.org/licenses/by/4.0/>).

Keywords: computational fluid dynamics; CFD; car aerodynamics; fan-driven downforce generator; peripheral jet; aerodynamic downforce

1. Introduction

It has been known for a long time [1–7] that the dynamics of a car improve significantly when additional aerodynamic forces are used to press the vehicle against the road. Many patents can be found [8,9] on the applications of various aerodynamic elements to improve the dynamics of fast cars. The articles [10–13] show how additional moving aerodynamic elements improve braking ability and safety during the braking process on a curved road. Additional aerofoils placed in front of and above the body [14] are used to increase the load on the front axle-driven wheels of cars used in Time Attack racing.

A quadratic dependence of the aerodynamic forces on the vehicle speed is a characteristic feature of all aerodynamic elements. This means the forces are too small at low speeds and too large at high speeds.

To compensate for this major disadvantage, the concept of sucking air from under the car has been used [15]. Ever since the beneficial effect of the aerodynamic downforce of a vehicle on its dynamic properties, especially during cornering, has been recognized in motorsport, there have been attempts to use fans to lower the air pressure under the body. Such a device allows to significantly increase the vehicle’s acceleration, reduce the braking distance, and extend the speed range for safe cornering.

An extreme case was Jim Hall’s Chapparral 2J car built for CANAM racing in the 1970s [16,17]. The air was drawn in by fans from a sealed area under the body (4.5 m², which was 3/4 of the total surface viewed from above) and later exhausted behind the

vehicle. A 45 horsepower auxiliary engine mounted behind the rear wheels powered two rear fans pumping 9650 cubic feet of air per minute ($4.55 \text{ m}^3/\text{s}$) at 6000 RPM. With the Chevrolet engine off, rumor has it, they could even push the car forward at 25 to 40 miles per hour (40–65 km/h). In theory, the Chaparral 2J could generate up to 11,000 N of downforce. Considering the area of 4.5 m^2 , this allows us to estimate the pressure under the car to be -2400 Pa . When the fans were turned on, the vehicle settled 5 cm on the suspension. With full fuel, the 2J could take corners at speeds that generate lateral accelerations of 1.25 to 1.5 g. The car had an incredible grip from zero traffic speed, allowing it to take corners at tremendous speed, and providing excellent acceleration and braking abilities. During qualifying, passing times were up to two seconds shorter than the competition. However, the car never won a race, often due to fan drive failures. Reliability proved to be an issue.

Perhaps the most challenging feature of building a working car with a fan that generates a low pressure under the body is the design of moving seals around the sucked-up portion of the chassis. In the case of the Chaparral 2J car, sealing curtains were mechanically coupled to the movement of the suspension to maintain a constant 1 inch (25.4 mm) clearance.

In 1978, the Brabham BT46B appeared, which used a horizontal rotor fan to cool the engine [18]. This fan, in addition to the air drawn from holes in the upper part of the body, also drew air from under the body. The underbody had a wide base sealed around the perimeter with spring plates positioned obliquely to the roadway. It is difficult to estimate what was the share of air sucked in from under the body in relation to that drawn from above in the entire stream of air flowing through the fan. In any case, the constructors expected the effect of lowering the pressure under the body, due to the fan.

The problem of effective sealing between the body and roadway also occurred later in the era of the use of the ground effect in the Lotus 78 and 79 designs. These vehicles used the ground effect to generate low pressures under the convex undersides of pylons located on the side of the body in the space between the front and rear wheels. Construction details of several versions tested on Lotus cars are known [19]. Lotus T78 brush skirt was made of nylon hair. Lotus T78 “suck-up” skirt was a flexible polyethylene plate set from the vertical so that the resulting low pressure lifted the lower edge of the plate—the skirt. The Lotus T78 “suck-down” skirt with the ceramic rubbing strip was an aluminum plate with a ceramic end, set so that the pressure difference caused the lower end of the strip to be pressed against the roadway. The Lotus T79 “board in the box” skirt comprised of rigid vertical plates which were moved up and down in slides in the body pocket, pressed against the carriageway by springs.

Due to their unreliability, however, the use of movable “skirts” was prohibited. Movable curtains had to provide a constant degree of sealing throughout the entire racetrack, regardless of bumps, pebbles, or other road surface disturbances. If the moving curtain seal was unreliable, it could cause the car to suddenly lose aerodynamic downforce and generate uncontrolled vehicle movement. This was the reason for excluding this solution from racing.

The problem of maintaining a constant distance of aerodynamic elements from the carriageway also occurred in F1 in the form of dependence of the characteristics of additional airfoils on their variable distance from the carriageway during the race resulting from the flexing of the elastic suspension.

The solution turned out to be the active suspension system [20]. After 11 years of development of this solution by Williams and later Lotus, in 1993, its use was prohibited [21], even though highly efficient systems were obtained. The main reason was the unwillingness of other F1 teams to bear the costs of developing this system. It is believed that this decision stopped the development of F1 for years and closed the flow of this technology to the automotive industry. This solution is currently used in many modern cars. The list of all 2007 vehicles with this feature can be found in the publication [22].

The primary problem of cars that generate low pressure under the body is air leakage from the outside. Designers have used various types of mechanical curtains at the body perimeter.

This paper focuses on analyzing the operation of air curtains in a configuration opposite to that used in hovercraft design solutions. The authors are unaware of any examples of using such solutions in car structures. However, an unusual application of the air curtain can be found in the virtual spoiler used in the design of the Aston Martin DB 11 car [23]. A virtual curtain generated at the end of the body causes an increase in pressure in front of it, producing a real downforce over a large body area.

It has been assumed that sealing the perimeter of the area from which air is drawn can be achieved by a curtain in the form of a flat stream of air directed vertically or obliquely downwards and outwards. The inertia of the high-speed air stream was intended to make it possible to maintain a negative pressure under the car. The studied device is referred to as the fan-driven downforce generator (FDDG). The work aimed to check the potential possibilities of using air curtains instead of mechanical curtains. To not complicate the analyzed structure with details of the fan's construction, it has been assumed that, hypothetically, the fan's work can be replaced by a pressure jump on the plane representing the fan's position. Simulations were therefore limited to simulating the flow induced by a simplified fan model. The use of invisible but physically existing air curtains involved their interaction with other body components.

2. Materials and Methods

2.1. The Basic Theory of Periferial Jet

The problem of determining the performance of the air curtain became of interest to engineers when vehicles on air cushions were developed. Air cushion vehicles are well known. There are various techniques to seal the cushion near the ground. One of the interesting ones is called peripheral jet.

The idea of an air curtain is presented in Figure 1a, and it is shown in the context of a car in Figure 1b. There are two zones characterized by different pressures, P_1 and P_2 . These areas are separated by an air curtain of height H and are supplied from the source of air at pressure P_0 through a nozzle of width b , where the nozzle is inclined at an angle α to the ground. Internal velocity v_1 and external velocity v_2 are present due to the different outlet pressures.

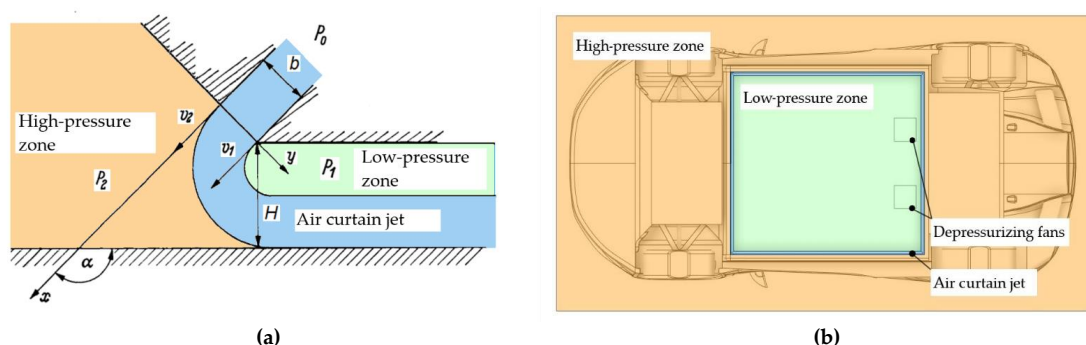


Figure 1. Air curtains: (a) schematic diagram; (b) sample placement under a vehicle.

There is a relationship between pressures, known as pressure coefficient:

$$C_p = \frac{p_2 - p_1}{p_0 - p_1} \quad (1)$$

Knowing C_p and pressures p_1 and p_2 , one can calculate required pressure p_0

$$p_0 = p_1 + \frac{p_2 - p_1}{C_p} \quad (2)$$

There are analytical solutions for non-viscous fluid flow in a curtain separating two areas with different pressures [24–26]. Data is typically presented in graphical form as shown in Figure 2. The comparison pressure coefficient C_p was calculated using inviscid and incompressible fluid flow, mixing theory, and compressible fluid flow (Mach number equal 0.51, 0.75 and 0.94).

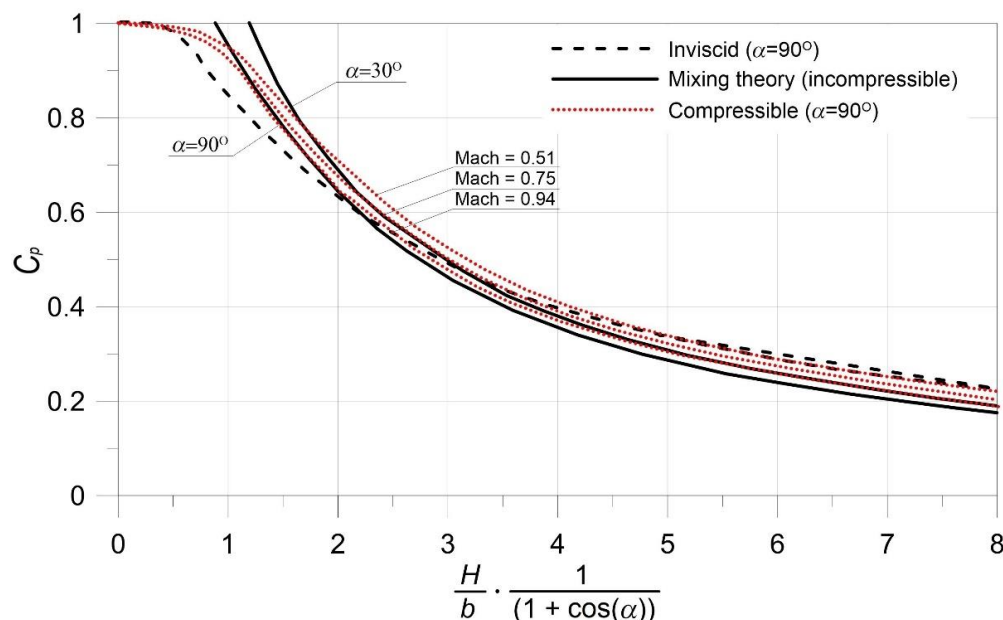


Figure 2. Comparison of pressure coefficient C_p calculated using inviscid and incompressible fluid flow, mixing theory, and compressible fluid flow [24–26].

One can determine the allowable pressure difference $p_2 - p_1$ that can be sustained at a given pressure p_0 , with a known ratio of curtain height to width H/b and the angle α of the initial curtain nozzle axis position. For a constant nozzle angle α , the pressure coefficient’s C_p value decreases with an increasing height to width ratio H/b .

This paper attempts to determine the feasibility of realizing such an “inverted air cushion” with numerical calculations. Air curtains would replace movable rigid curtains. The purpose of the curtains would be to seal the low-pressure region under the largest possible area of the car.

2.2. CFD Methodology

The model was developed with a computational fluid dynamics (CFD) code ANSYS Fluent 2022R1, in which incompressible Reynolds-Averaged Navier–Stokes (RANS) equations were solved using a finite-volume method. Using the Einstein summation convention, the continuity equation takes the form of:

$$\frac{\partial \bar{v}_i}{\partial x_i} = 0 \tag{3}$$

and the momentum conservation equation can be written as:

$$\rho \left(\frac{\partial \bar{v}_i}{\partial t} + \bar{v}_j \frac{\partial \bar{v}_i}{\partial \bar{v}_j} \right) = \rho f_i + \frac{\partial}{\partial x_j} \left[-\bar{p} \delta_{ij} + \mu \left(\frac{\partial \bar{v}_i}{\partial x_j} + \frac{\partial \bar{v}_j}{\partial x_i} \right) - \rho \overline{v'_i v'_j} \right] \tag{4}$$

where v_i represents the i -th component of velocity at a point x_i in space, ρ is the fluid density, f_i is the body force (e.g., gravity), p represents the static pressure, μ is the dynamic viscosity, δ_{ij} is the Kronecker delta, bars denote mean values, and apostrophes represent instantaneous values. Because of the Reynolds stress tensor $-\rho \overline{v'_i v'_j}$, the closure problem

arises, and additional equations are needed. They are supplemented by turbulence models, which can be roughly categorized in two basic groups: models that solve transport equations for Reynolds stress tensor components, and models that follow the Boussinesq hypothesis and introduce turbulent viscosity. The turbulence model selected for this work belongs to the latter group. It is assumed, that the Reynolds stress tensor is proportional to the mean strain rate tensor:

$$-\rho \overline{v'_i v'_j} = \mu_t \left(\frac{\partial \bar{v}_i}{\partial x_j} + \frac{\partial \bar{v}_j}{\partial x_i} \right) \quad (5)$$

where μ_t is the turbulent viscosity. The shortcoming of turbulence models based on turbulent viscosity is that they fail to predict strongly rotating flows, strongly decelerated flows, or curvature effects. Nevertheless, they were validated in car aerodynamic analyses with satisfying results [27]. For this study, a realizable k - ϵ turbulence model [28] was used.

A disadvantage of standard two-equation turbulence models such as k - ϵ is the excessive generation of the turbulence energy in the vicinity of stagnation points [29]. For this reason, a production limiter was added to the source term G_K in the transport equation of turbulent kinetic energy k .

$$G_k = \mu_t S^2 = \min(G_k, C_{lim} \rho \epsilon) \quad (6)$$

where S is the magnitude of the strain rate, ϵ is the turbulence dissipation rate and C_{lim} was a constant equal to 10.

Enhanced wall treatment was used as a near-wall modelling method. A pressure-based solver, implicit formulation, and Green-Gauss node option for calculating gradients were used for all the studied cases. The coupled pseudo-transient scheme was applied for pressure-velocity coupling. Second-order spatial discretization was set for pressure and momentum.

Forces and moments acting on the geometry components were monitored throughout the iterative calculation process. If oscillations were captured, then iterative calculations were run until 5–10 periods of stable oscillations were captured.

In every studied case, the downforce was calculated as a vertical component of pressure and viscous forces acting on the walls. The power was calculated as a product of the volumetric flow rate and the pressure difference generated by the fan.

3. Results and Discussion

3.1. CFD Analyses of a Two-Dimensional Stationary Air Curtain

In this subsection, results from two-dimensional planar air curtain models are shown for the case of a stationary vehicle. The computational domain was limited to the area around the air curtain, as shown in Figure 3.

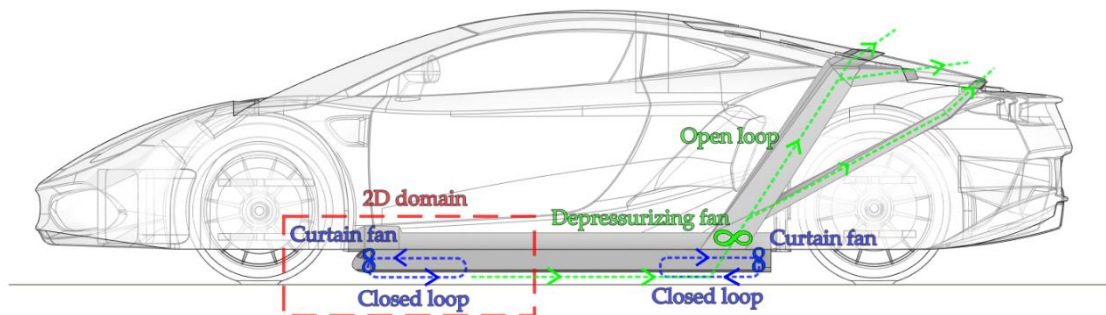


Figure 3. Computational domain of a planar 2D model in the context of a car model.

3.1.1. Curtain Height Considerations

The height of the air curtain is a significant parameter. From a practical point of view, the curtain must be tall and thin. Unfortunately, as shown in Figure 2, the H/b ratio defines the maximum pressure difference that the air curtain can sustain. Figure 4 shows how the velocity distribution in the air curtain varies with its height (10 mm, 20 mm, 30 mm, 40 mm, 50 mm) at a constant fan pressure increment of 1000 Pa.

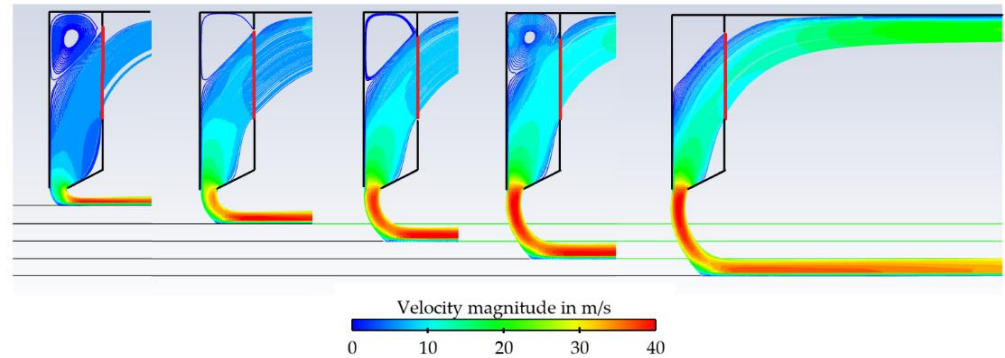


Figure 4. Velocity values on pathlines passing through a fan with a constant pressure increment of 1000 Pa for different curtain heights (from the left: 10 mm, 20 mm, 30 mm, 40 mm, 50 mm) and nozzle width of 10 mm.

Figure 5 shows the respective changes in downforce. Analogous to the C_p curve shown in Figure 2, after a certain height the downforce curve starts to flatten, and the curtain can be moved further away with a relatively small loss. Above the height of 50 mm, the downforce decrease is approximately 2 N of downforce per 1 mm of height. Smaller sensitivity to changes in height also means that disturbances in the form of uneven ground surface would be less harmful.

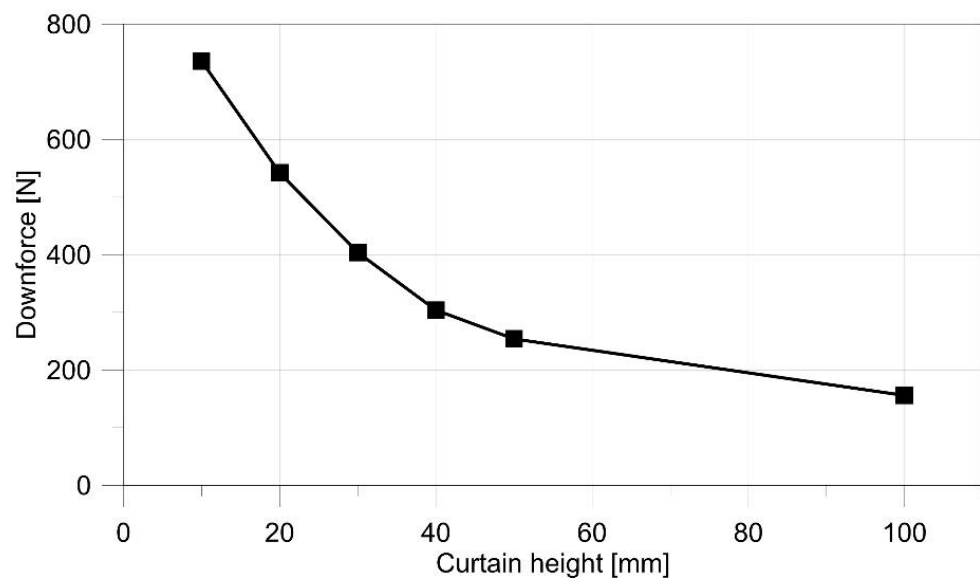


Figure 5. Variation of generated downforce with constant fan pressure in function of the curtain height.

After preliminary tests of the 2D simulation model of the curtain segment, it was decided to use height of the curtain equal to 50 mm, assuming a 10 mm nozzle width. Considering the functions shown in Figure 2, for a ratio of $H/b = 5$ and $\alpha = 90^\circ$, a C_p value of about 0.3 can be expected.

In this work, it was considered that providing a curtain height of 50 mm would be equivalent to the performance of the mechanical curtain with 25.4 mm clearance. In the

case of Chaparral 2J, the mechanical curtain surrounding the vehicle was positioned at the height of 25.4 mm above the ground [16].

3.1.2. Curtain-Only Variant of FDDG

The first system which has been adopted generates the air curtain in a closed loop. The air circulation scheme which was used in CFD simulations is depicted in Figure 6, which shows a 2D planar model of a cross-section of a curtain. The area is surrounded by a pressure outlet condition to the environment, which automatically changes to a pressure inlet when the flow direction changes; the upper wall surface of the high-pressure chamber, the upper wall surface of the low-pressure chamber, and the surface are treated as a symmetry surface. At the bottom, there is a stationary ground surface. The low-pressure chamber area is equal to 0.8 m^2 .

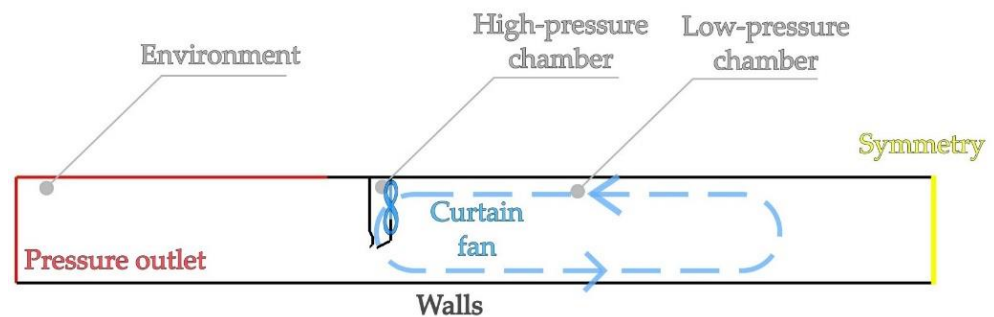


Figure 6. Scheme of the planar 2D model of the curtain-only variant of FDDG.

Figure 7 contains velocity and pressure contours. The fan takes the air from the inside of the low-pressure chamber and, by increasing its pressure, transfers it to the curtain nozzle supply chamber. The result is a constant reduced pressure in the low-pressure chamber with recirculation of air by the fan.

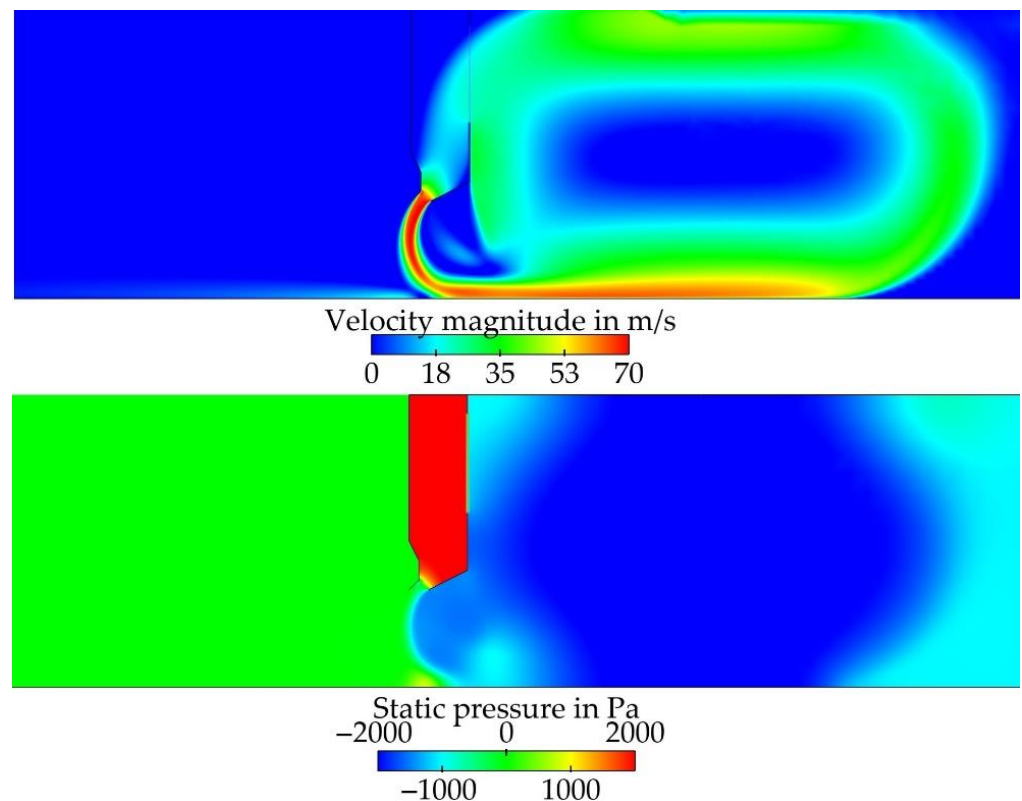


Figure 7. Velocity and pressure contours in the curtain-only variant, for curtain fan $\Delta p = 3000 \text{ Pa}$.

Figure 8 presents the basic characteristic of this version of the FDDG. With increasing curtain fan pressure, the downforce to power ratio decreases. The subsequent versions of FDDG studied in the paper showed improved performance.

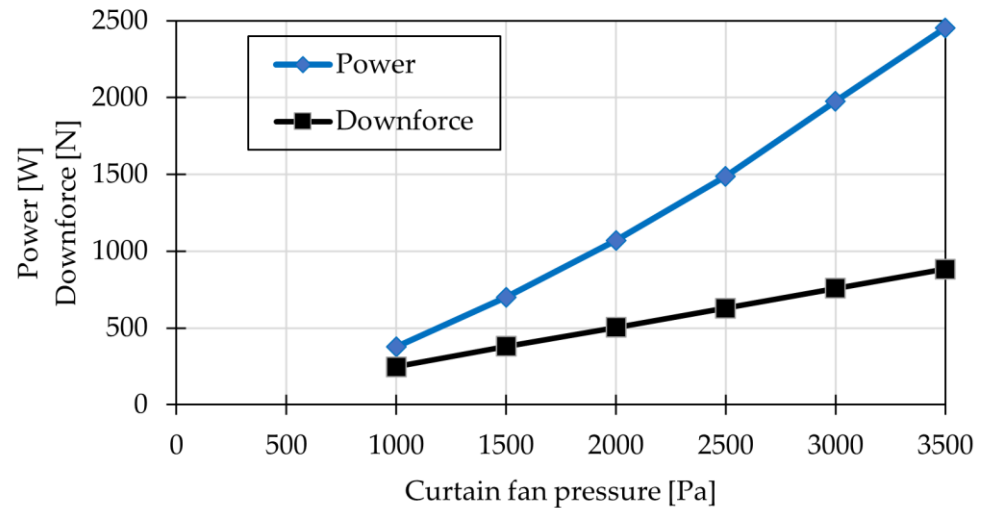


Figure 8. Downforce generated by curtain fan and required power as a function of the curtain fan compression.

3.1.3. Curtain with Depressurizing Fan

The second version of the FDDG is more complicated. It contains two circuits, where one fan is realizing the circulation in the curtain and the second fan is controlling vacuum pressure in the chamber, as shown in Figure 9.

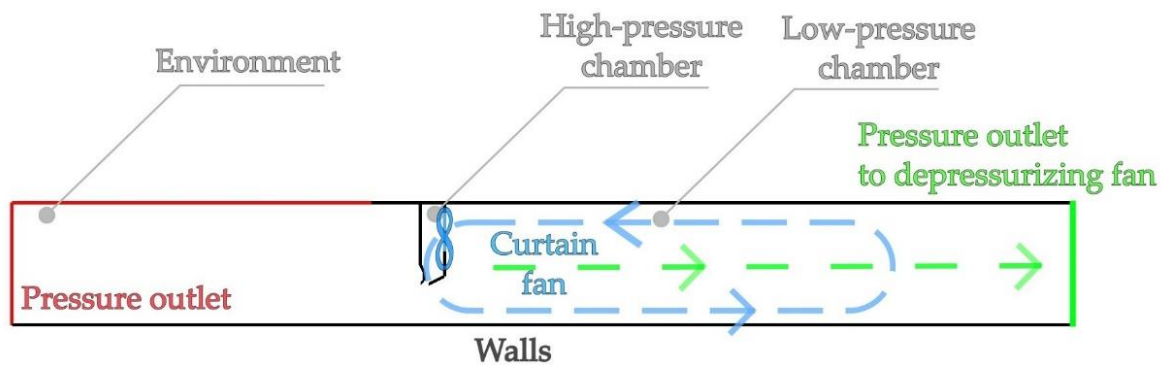


Figure 9. Scheme of FDDG with air curtains and depressurizing fan.

Figure 10 shows velocity and pressure contours. In the case of generating an air curtain only, the structure of the air curtain flow from the outside was simple: air flows down from the top and is rejected to the side. In the case of generating an air curtain and depressurizing the chamber with an additional fan, the flow structure is somewhat more complicated: air is drawn in from the outside of the air curtain, partly used to create the air curtain, and partly expelled outside of the low-pressure chamber.

Similar downforces may exist for two different parameter settings for the recirculation fan and the depressurizing fan. Figure 11 presents the basic characteristics of this FDDG version. It can be seen that the power required to keep the air curtain active changes only slightly. The reduction of pressure in the chamber is due to the operation of the depressurizing fan.

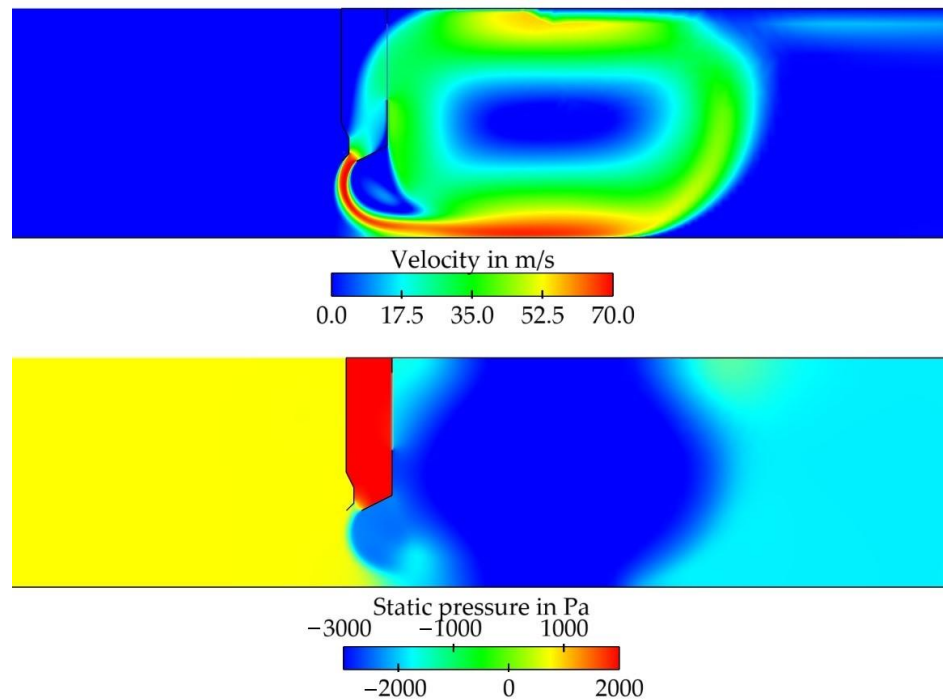


Figure 10. Velocity and pressure contours for the FDDG with air curtain and depressurizing fan, with curtain fan $\Delta p = 3000$ Pa and pressure at the outlet to depressurizing fan $p = -1000$ Pa.

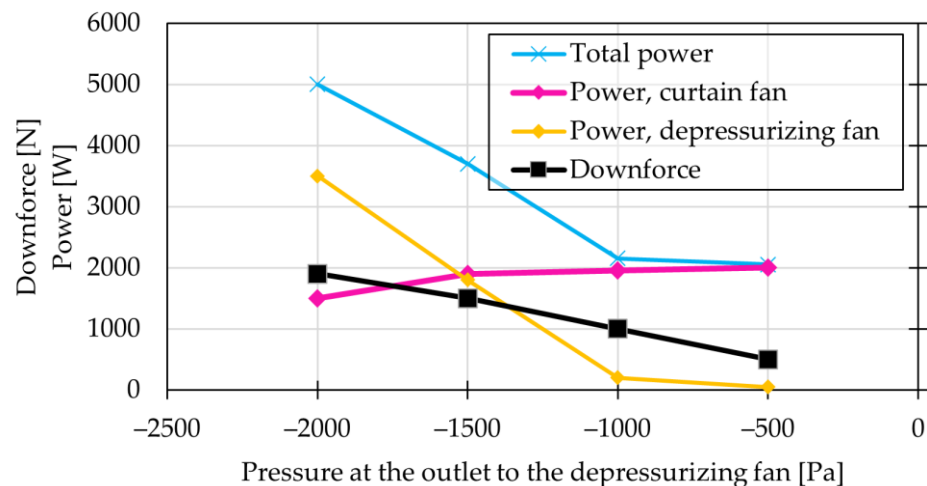


Figure 11. The downforce generated by FDDG and the required power with air curtains and depressurizing fan running as a function of the depressurizing fan compression. The air curtain fan was operating at constant $\Delta p = 3000$ Pa.

3.2. CFD Analyses of a Three-Dimensional Moving Air Curtain

Two-dimensional models were sufficient for the preliminary study of a stationary vehicle. To apply the presented idea to real cars, three-dimensional air curtains are needed. The air curtains on vehicles move in relation to the surrounding air, as well as relative to the ground, and they undergo some deformation during movement. This problem was considered in the work [30] devoted to the deformation of the air curtain during the hovercraft disk vehicle motion. The vehicle moved on an air cushion created under it, sealed at the perimeter just by the air curtain. In our case, the low-pressure chamber sealed at the perimeter by the air curtain must move at the speed of the vehicle in one of the directions. Therefore, on a rectangular perimeter such as the air curtain, completely

different ambient conditions occur on the curtain surfaces perpendicular to the direction of motion than on surfaces parallel to it.

The curtains can take any shape, but in the case of cars, a rectangular shape allows to take advantage of the large underbody area. Therefore, it is assumed that the chamber would have a rectangular shape viewed from the top.

In the model of the FDDG, there are air curtains on each side of the low-pressure chamber. One at the front in the direction of movement, one at the rear, and two at the side closures that are parallel to the direction of movement. There is also a fan in the ceiling of the chamber that sucks the air out of the interior of the chamber. In Figure 12, the FDDG shell is presented.

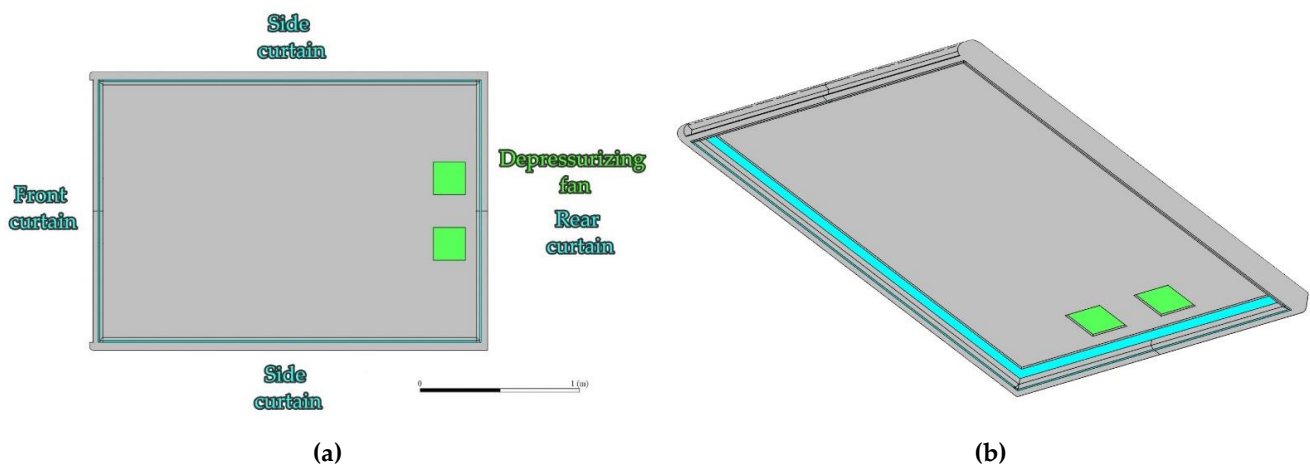


Figure 12. Geometry of the shell object of FDDG used for 3D CFD simulation of the moving object: (a) bottom view; (b) angled view from bottom.

Figure 13 presents velocity vectors at nozzle outlets when the FDDG shell moves to the left with a speed equal to 40 m/s, generating almost 2000 N downforce. Irregularities at both the front and rear corners can be observed.

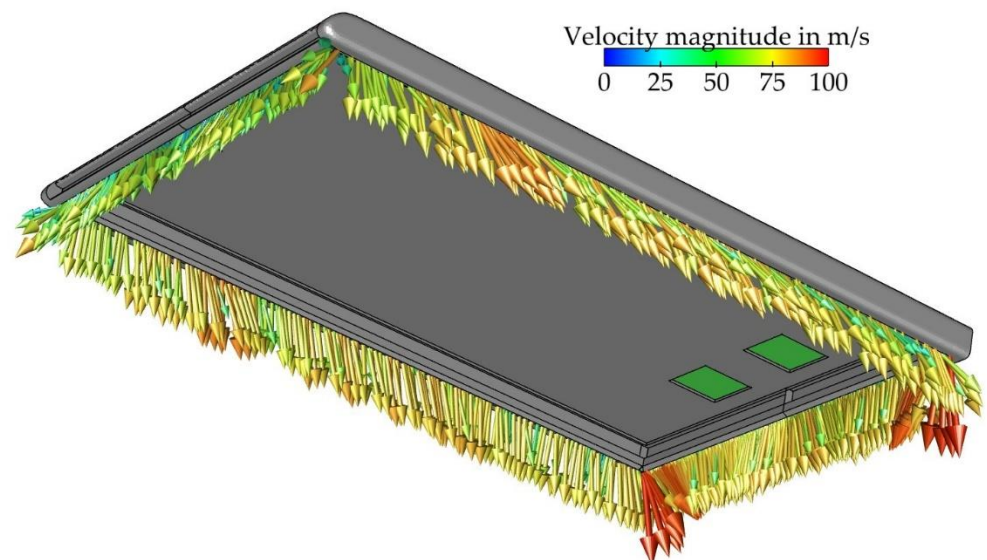


Figure 13. Velocity vectors at curtain nozzles, seen from the bottom, on a half part of the shell object traveling at speed of 40 m/s.

3.2.1. Discussion of Various FDDG Variants

Two ways of generating aerodynamic downforce were considered during previous 2D analyses. Only by using the curtain fans, or additionally using a depressurizing fan

that draws air from the air-curtain-protected area. Figure 14 shows a comparison of the magnitude of the generated downforce for both of these configurations as a function of the velocity of the 3D shell object motion.

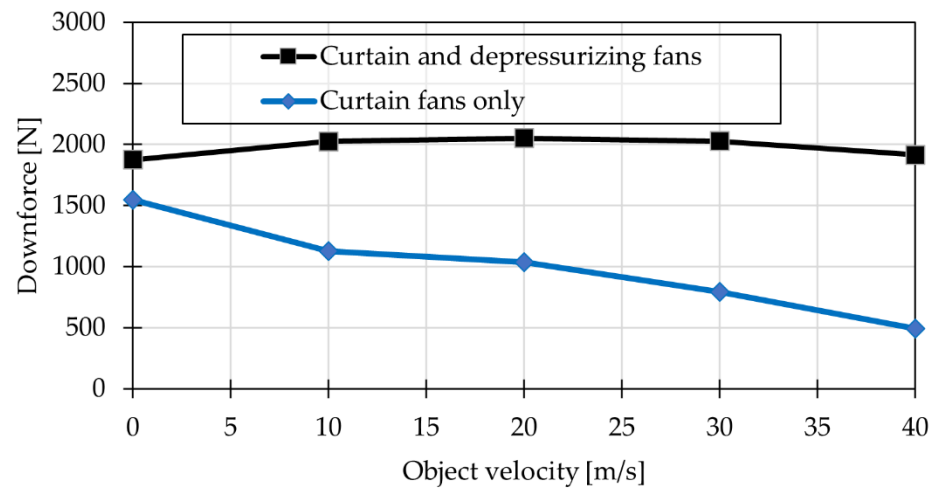


Figure 14. Comparison of the aerodynamic downforce achieved using only the air curtain fans and additionally supported by the depressurizing fan.

It can be seen that at zero motion velocity, the differences are only due to the difference in the areas of the two types of fans. On the other hand, the effectiveness of the pressure force generation by only the air curtain fans decreases significantly with the object's velocity.

As indicated earlier, the primary disadvantage of air curtains is their strong dependence on the curtain height. The effectiveness of an air curtain depends on the ratio between the height and the width of the air curtain nozzle, as well as the air discharge velocity.

As shown in Figure 15, in order to increase the height of the curtain while maintaining the same downforce, either the nozzle discharge width can be increased at the same nozzle supply pressure, or the discharge velocity can be increased at the same nozzle width. In both cases, this involves an increase in the flow rate through the nozzle and an increase in the energy consumed by the fan supplying the nozzle.

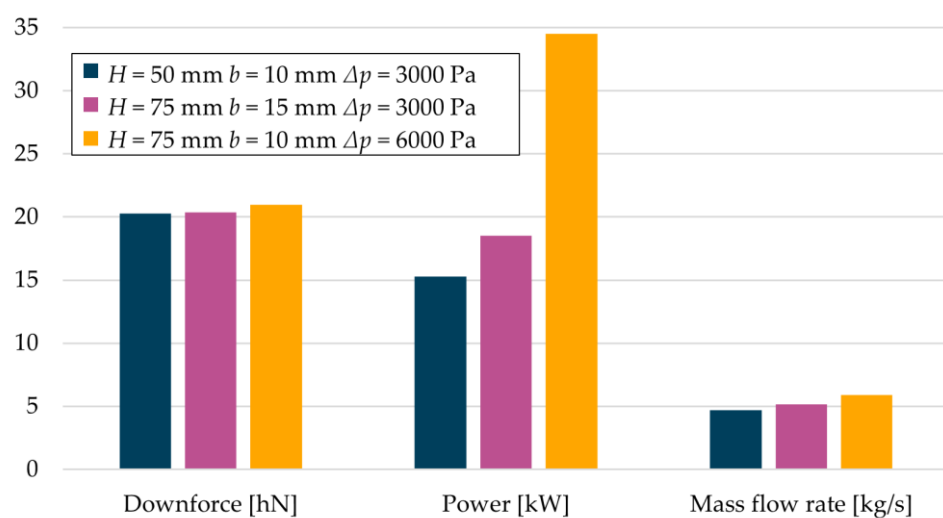


Figure 15. Conditions needed to change curtain height from 50 mm to 75 mm for the same aerodynamic downforce generated.

Air curtains are a necessary element for the effective operation of the FDDG. Figure 16 shows the changes in generated downforce under a 3D shell object moving at 40 m/s. The main fan generates a pressure jump of 3000 Pa, sucking the air out of the low-pressure

chamber. The result of turning the curtains off is shown. With a curtain height of 50 mm, the operation of only the main fan ejecting air from the chamber to the outside does not generate the expected aerodynamic downforce.

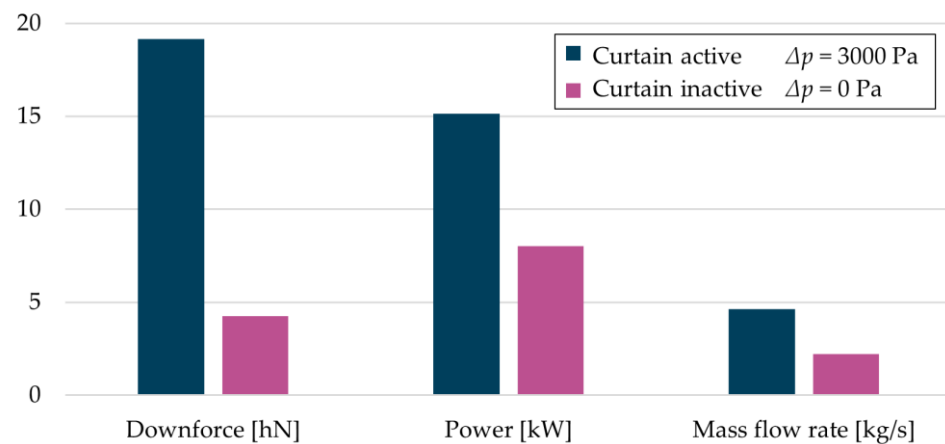


Figure 16. Comparison of operation parameters in the case with active curtain and curtain deactivated.

3.2.2. Taking Advantage of the Stagnation Pressure

As the object moves at a certain velocity, the air is trapped at the front surface of the object, causing the pressure to rise to the total pressure. The front curtain nozzle can be fed by a supporting fan, drawing air from this area, or by a circulation fan located on the back wall of the nozzle, drawing air from the low-pressure chamber as can be seen in Figure 17.

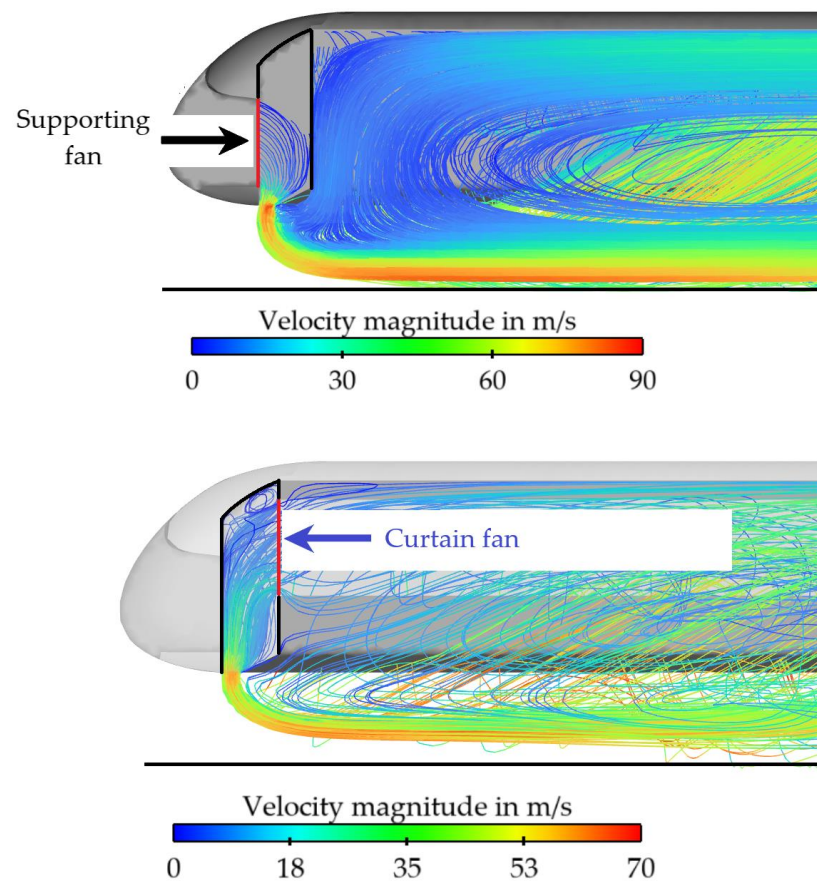


Figure 17. Scheme of operation of the supporting fan and circulation fan.

Figure 18 shows the differences in the values of the aerodynamic downforce generated by an object moving at different speeds in the configuration when the air curtain is active and when its role is taken over by the supporting fan. It can be seen that with increasing speed, the aerodynamic downforce increases due to the supporting fan utilizing the dynamic pressure on the front wall of the chamber. However, this happens only up to a speed of 30 m/s. After that, other physical phenomena prevail. Air from the front enters the low-pressure chamber through the front curtain.

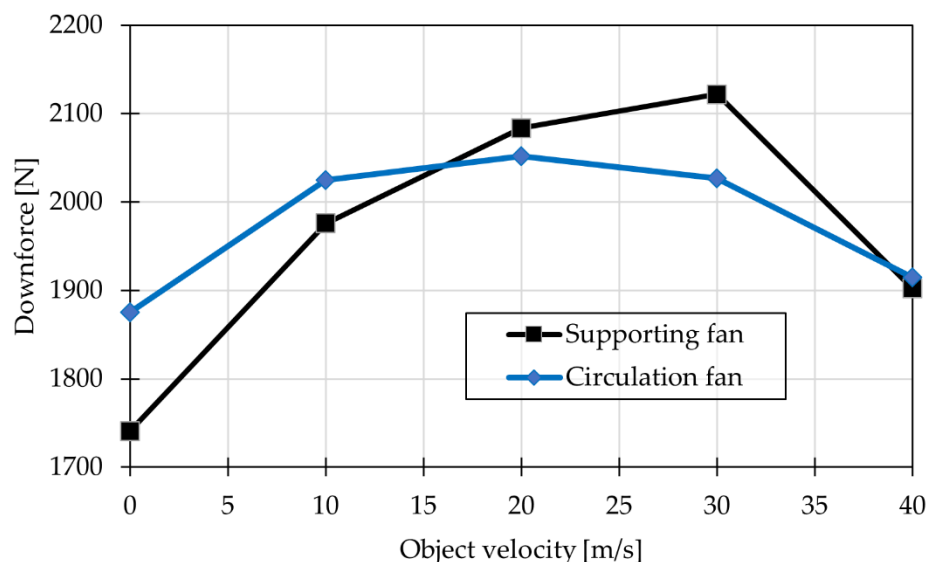


Figure 18. Variation of aerodynamic downforce values produced by a shell object moving at different speeds with the chamber front curtain fed by a supporting fan or circulation fan.

3.3. CFD Analyses of the FDDG in a Sports Car

Positive results from simulations of the performance of the three-dimensional shell objects moving at a fixed distance above the ground at different speeds, with the generation of aerodynamic force through fans, allowed for the construction and testing of a device that is part of a sports car. The analyzed geometry was a road version of a Polish supercar, Arrinera Hussarya. The presented geometry was not optimized for downforce. No splitter plate was present. There was a moderate diffuser and a moderate spoiler that could be hidden in the body outline (Figure 19a).

The FDDG was mounted at the undercarriage, leaving 50 mm clearance from the ground. Outlet ducts were routed from the fan to the upper outline of the car body with the idea of enhancing the aerodynamic downforce in the spoiler area (Figure 19b).

Domain size is shown in Figure 20. Velocity was specified at the inlet surface with a turbulence intensity of 5% and a length scale of 5 mm. Moving wall boundary conditions were applied to the ground and car wheels. Half of the geometry was modelled with a symmetry boundary condition. The same boundary condition was also applied to the side and top surfaces. Constant gauge static pressure of 0 Pa was applied at the outlet surface.

Meshes were generated in Fluent Meshing 2022R1. A relatively uniform surface mesh was generated on the car body (Figure 21). Mesh refinement in the region of high velocity and pressure gradients was provided by box-shaped bodies of influence (BOIs) around the car body and in the undercarriage area. A poly-hexcore algorithm was chosen for the volume mesh.

The boundary layer mesh was designed to fit the wall function approach. The boundary layer mesh consisted of five elements with a growth rate of 1.2 and a constant first layer height of 1.3 mm on the car body to achieve y^+ in the range of the logarithmic layer.

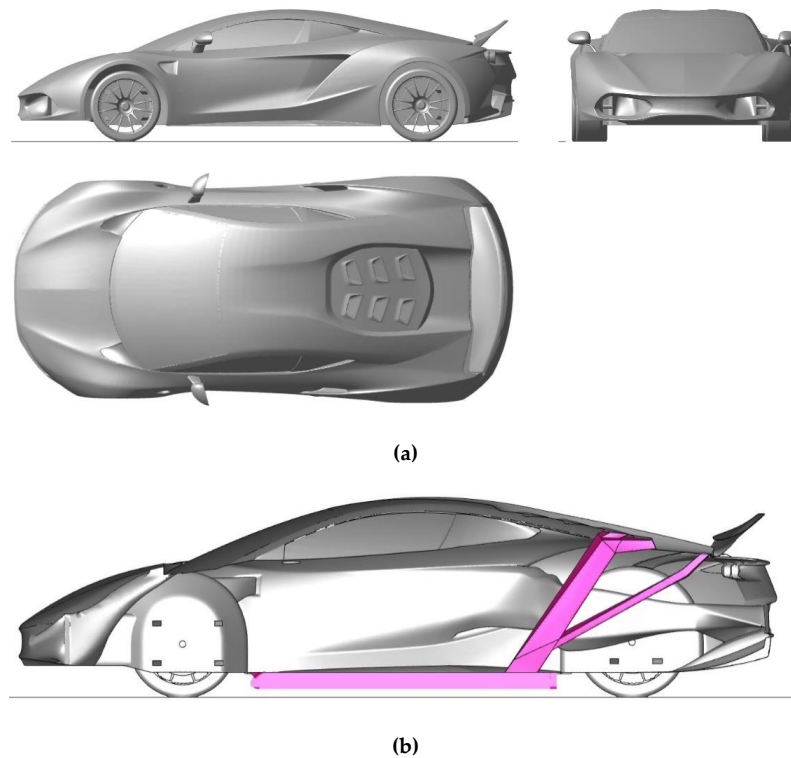


Figure 19. The geometry of the analyzed car: (a) Without the FDDG, different views; (b) With the FDDG marked in magenta, cross-section view.



Figure 20. Size of the computational domain with length $L = 4.6$ m height $H = 1.1$ m and width $W = 1.1$ m.

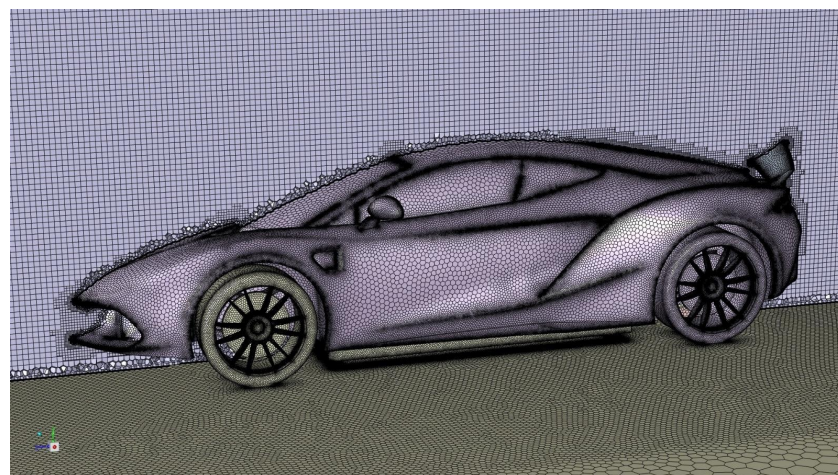


Figure 21. Computational mesh in a cross-section.

A grid sensitivity check for the car body used in the study was already reported by the authors in [14]. Grid convergence indexes of 0.1% and 2.4% were reported for drag and lift coefficients, respectively.

In this paper, additionally, a grid convergence test was performed for the undercarriage area, where large velocity gradients were present due to the fan action. Mesh refinement in the nozzle area is seen at the ground surface in Figure 22a,b. Three mesh sizes were prepared, where characteristic cell size in the undercarriage BOI was different by a factor of two (Figure 22c). Velocity magnitude contours for different mesh sizes in the nozzle area are shown in Figure 22d.

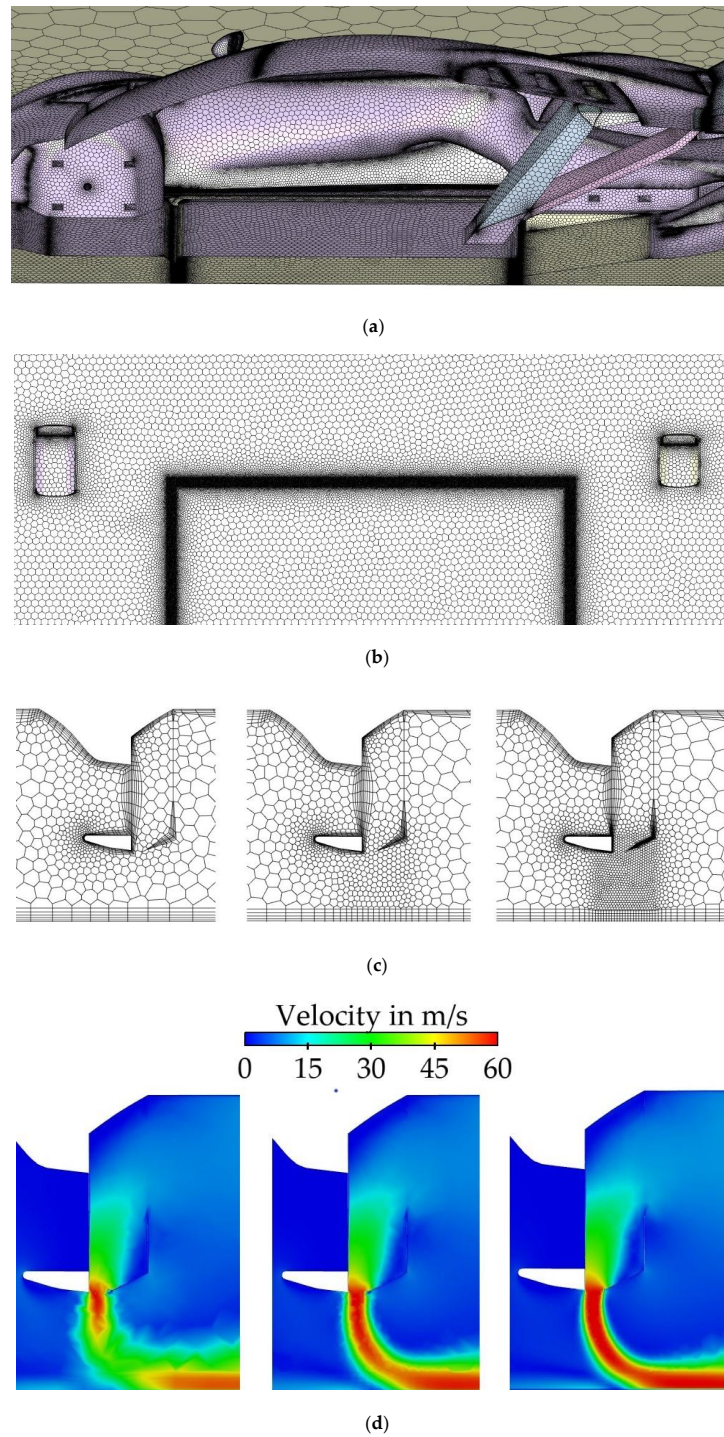


Figure 22. Grid convergence test in the undercarriage area: (a) Cross-section view, refinement in the proximity of curtains can be seen; (b) Ground view from the bottom; (c) Zoom at the front nozzle, various mesh sizes; (d) Velocity contours at the front nozzle for various mesh sizes.

Simulations were performed for all three meshes for the case of a stationary car and fans running at 3000 Pa. The monitored parameter was an aerodynamic downforce acting on the car, as well as a drag and volumetric flow rate through all the fans. As shown in Table 1, the relative differences of observed parameters did not exceed 2% after the first mesh refinement. The finest of the three meshes was selected for further studies. The final mesh comprised 9.5 million cells and had inverse orthogonal quality smaller than 0.9, which means a very good mesh quality.

Table 1. Grid convergence test results.

Parameter	Coarse Mesh	Medium Mesh	Fine Mesh
Cell count	7 mln	8 mln	9 mln
Force in the forward direction in N	87	86	84
	(+3.1%)	(+1.7%)	
Downforce in N	2541	2624	2629
	(−3.3%)	(−0.2%)	
Volumetric flow rate through all fans in m^3/s	5.81	5.79	5.70
	(+1.9%)	(+1.5%)	

3.3.1. Analysis of FDDG Performance

To evaluate the usefulness of the FDDG over a wide range of vehicle movement speeds, plots of the variation of generated aerodynamic forces as a function of vehicle speed are shown in Figure 23. In Figure 23a, the series denoting car downforce without the FDDG starts at zero and then exhibits a constant increase proportional to the velocity squared due to the action of aerodynamic elements. On the other hand, the car with an FDDG has a significant downforce even at zero speed. The downforce decreases with increasing speed. The reason for the complicated characteristics of the downforce curve with the FDDG is the simultaneous occurrence of many phenomena: the negative interaction of the FDDG with aerodynamic elements of the car, the interaction of front and side curtains, the non-ideal performance of the side curtains at high speeds, and the limits of pressure difference that air curtains can sustain. Overall, the device plays a useful role up to a speed of 45 m/s. The drag force is larger by 25% at this speed, as shown in Figure 23b. Interestingly, the car with an FDDG has a slightly lower drag at speeds (0–15 km/h), but it is of low significance in this speed range.

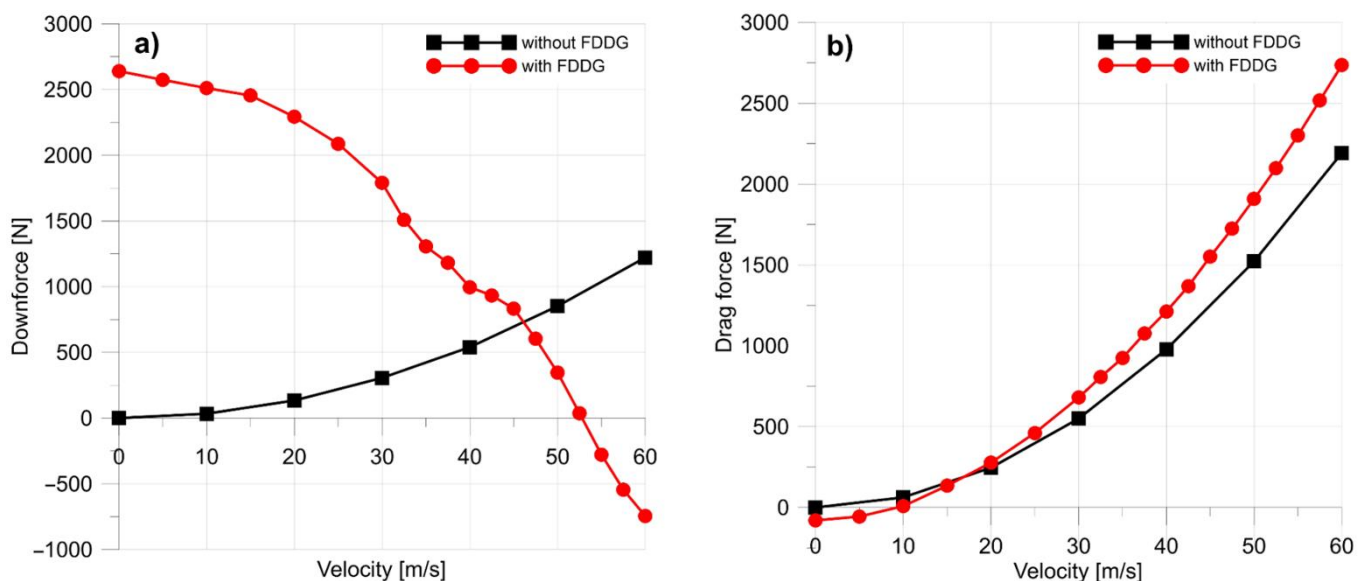


Figure 23. Aerodynamic forces for the baseline case and the case with FDDG for various inlet speeds: (a) Downforce; (b) Drag force.

As shown in Figure 24, the power required for operating fans (depressurizing fan and four curtain fans, one on each side) at 3000 Pa remains at a relatively constant 17 kW level regardless of the vehicle speed.

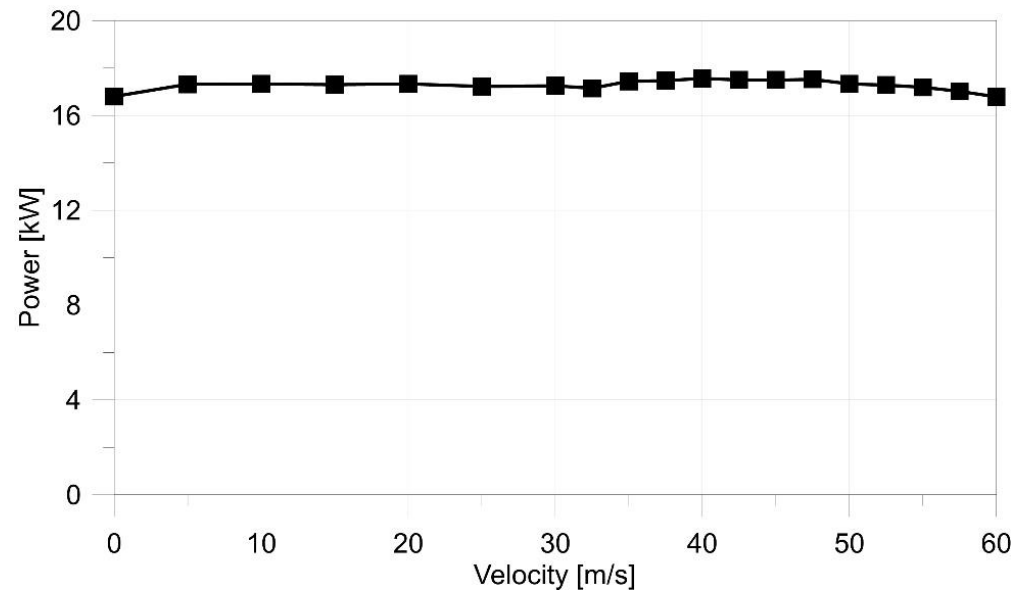


Figure 24. Power required for operating fans at $\Delta p = 3000$ Pa.

Figure 25 shows the pressure coefficient at the bottom surface and symmetry plane. The pressure coefficient was calculated using reference density $\rho = 1.225 \text{ kg/m}^3$ and velocity equal to inlet air velocity. A low-pressure region in the area surrounded by air curtains can be seen, which contributes to high downforce at low vehicle speeds. However, for the case without an FDDG, downforce is generated with increasing velocity due to the action of the underbody, diffuser, and spoiler. In the case with the FDDG, the diffuser is hidden in the wake of air curtain components and is not used effectively. Moreover, a massive stagnation region upstream of the FDDG can be observed. This is the main reason for decreased downforce at high speeds.

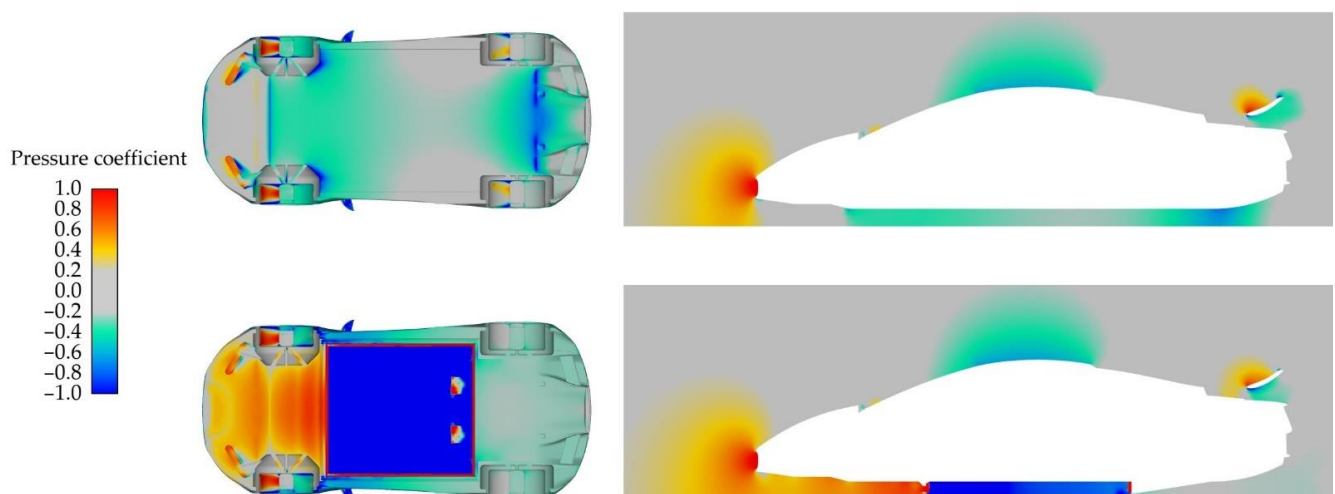


Figure 25. Pressure coefficient for inlet speed of 40 m/s, bottom, and symmetry views. (Top): without FDDG; (bottom): with the FDDG.

Figure 26 shows the problem of the buildup of high static pressure in the front area for the case with the FDDG for increasing velocities. This issue could be addressed by modifying the geometry of the front of the car.

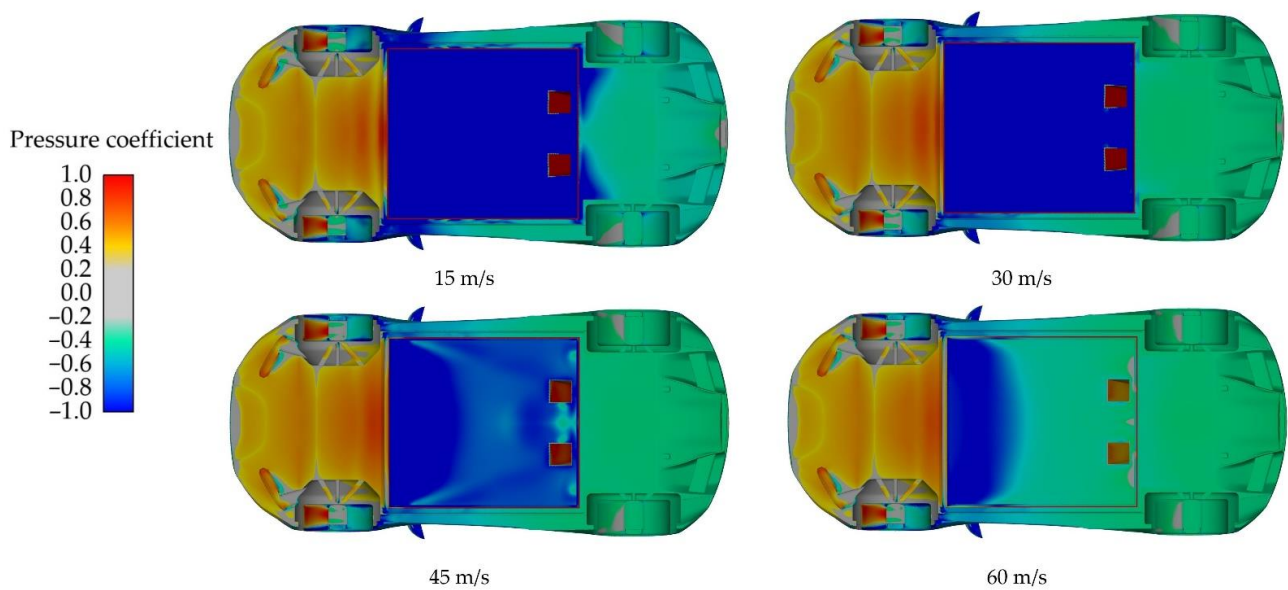


Figure 26. Pressure coefficient at the bottom surface for the case with fans turned on for various inlet speeds.

The effect of the recirculation fans is shown in Figure 27, containing the pressure distributions on the car surface, when the fans are not operating and when they are active. When curtain fans that produce air curtains separating the interior of the low-pressure chamber from the surroundings are not operating, the depressurizing fan system does not produce negative pressure in the chamber under the car. Without air curtains, the car did not generate almost any downforce, while after turning curtain fans on, a downforce of 2300 N was captured. At the same time, turning on the curtain fans did not increase the drag force substantially (6% increase).

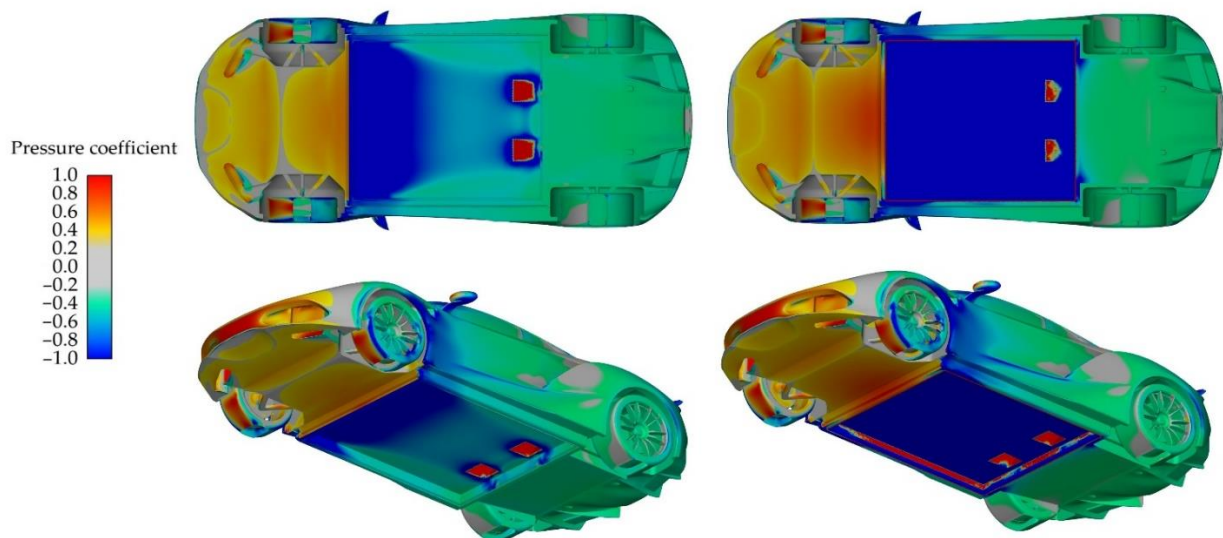


Figure 27. Pressure coefficient for the inlet speed of 20 m/s. On the (left), circulation fans generating air curtains were deactivated; on the (right)—they were active.

Pathlines released from the front curtain fans can be seen in Figure 28 in a cross-section view. The curtain is sucked into the low-pressure zone and the proportion of air entering the chamber under the front nozzle increases for increasing speed.

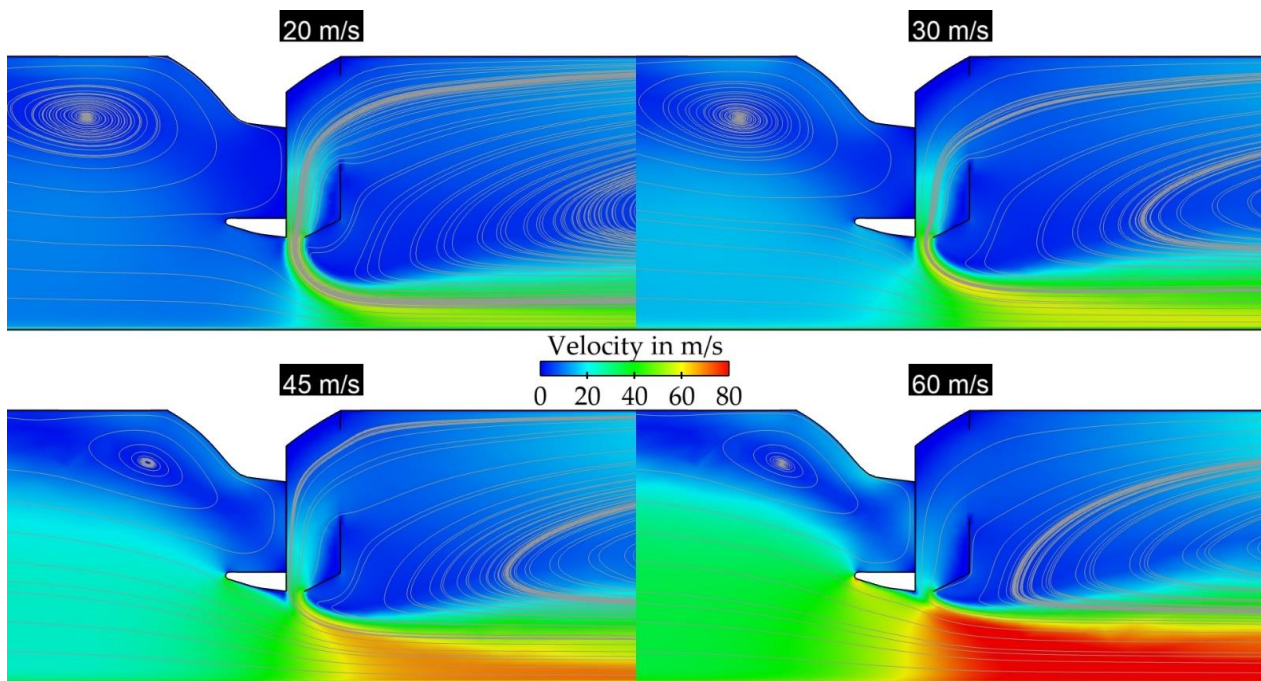


Figure 28. Velocity distribution and pathlines at front nozzles of FDDG for various inlet velocities.

In Figure 29, pathlines from all curtains are shown, and their interaction within the low-pressure chamber is clearly visible. The flow pattern inside the low-pressure chamber will vary with increasing vehicle speed.

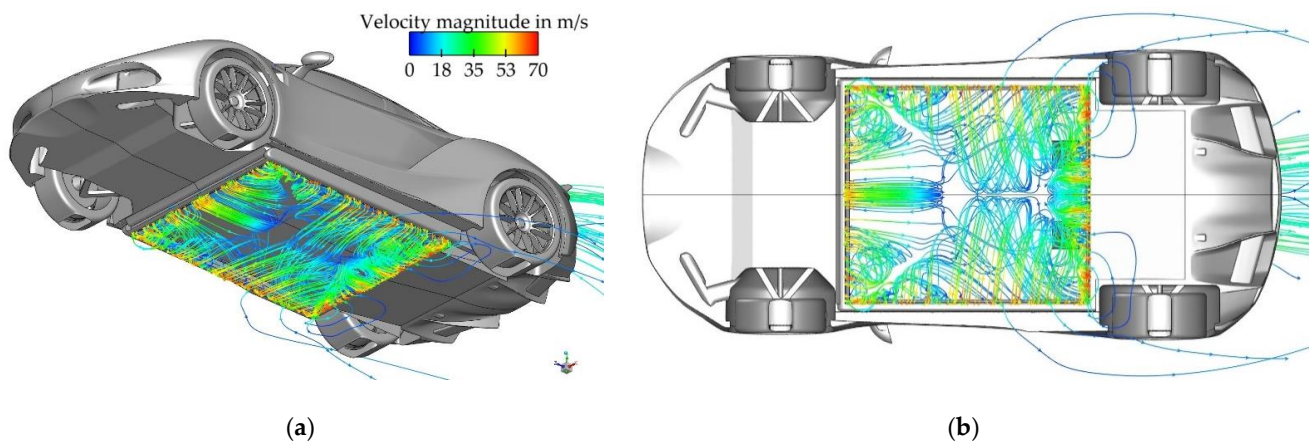


Figure 29. Pathlines released from the fan surfaces for inlet velocity of 20 m/s. (a) Angled view from bottom; (b) Bottom view.

3.3.2. Further Optimization Directions

In the course of analyses, many opportunities for further optimization of the system were discovered.

One can take advantage of the stagnation region in front of the car and switch from the curtain fan to the supporting fan for high car velocities, as shown in Figure 30. This was tested before in a 3D example of a shell object, and it also proved to be a viable approach in the case of a full car model, as it increased downforce by 5% for the same fan power.

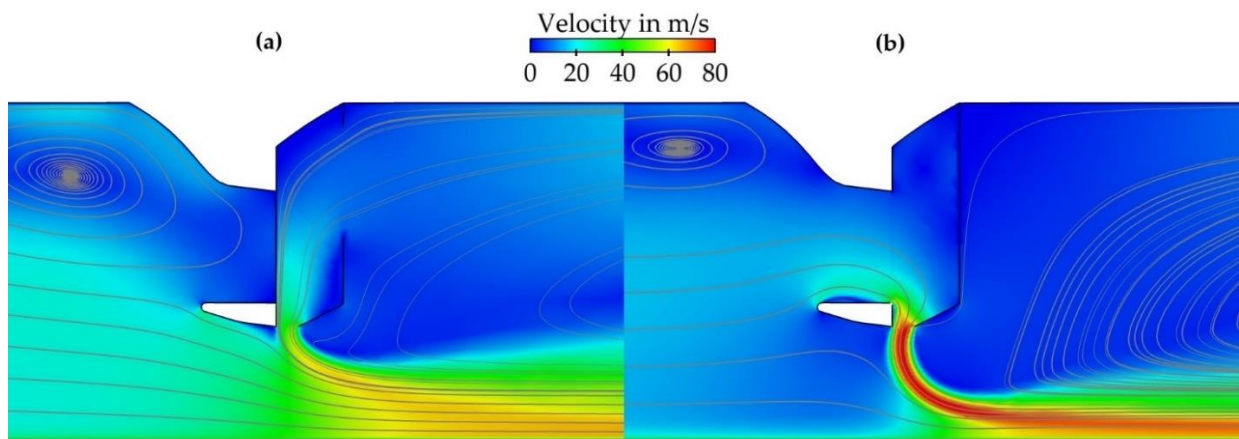


Figure 30. Velocity distribution at front nozzles of the fan-generating device for inlet speed of 40 m/s. (a) Air curtain fan active; (b) Support fan active.

Another potential for optimization lies in the management of ejected air. The ejected air can be used to interact advantageously with classic aerodynamic elements, such as flaps or spoilers. In the studied case, the airflow was directed through three ducts, one of which supplied the air under the rear spoiler, as shown in Figure 31. Reduced pressure on the lower spoiler surface is clearly visible in Figure 32, which attributes to increased downforce on the rear axle.

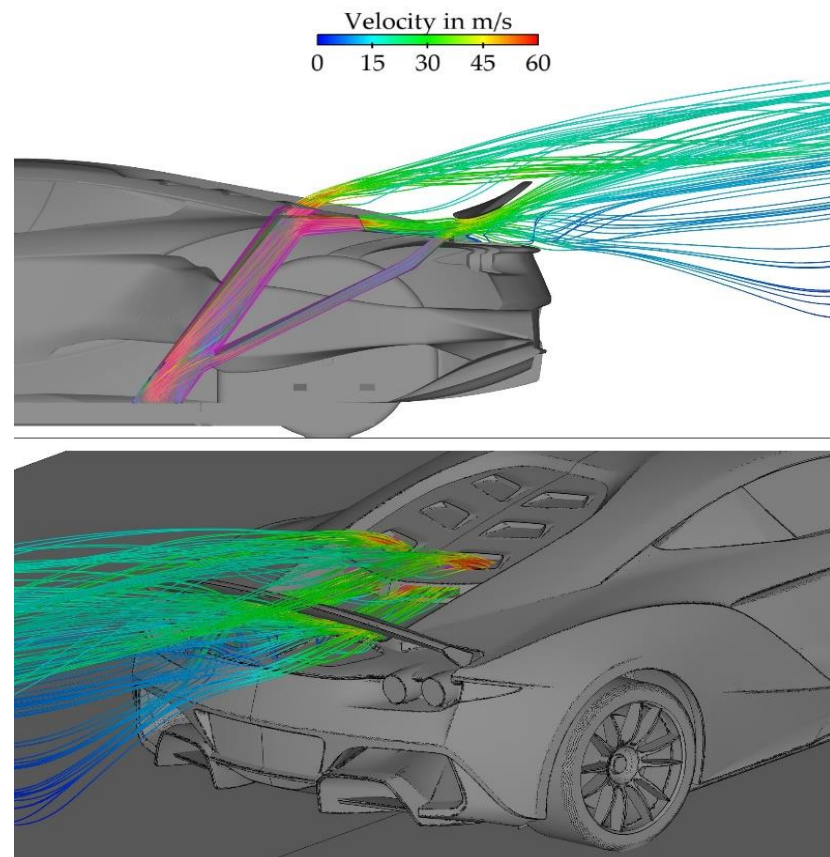


Figure 31. Pathlines of air exhausted from the main fan through the outlet ducts.

The shape of the ducts from the depressurizing fan also contribute to the effectiveness of the FDDG. Due to pressure losses, not all of the pressure from the depressurizing fan is used to generate downforce; some is inevitably lost. A test was conducted where an artificial atmospheric outlet for air was created just downstream of the depressurizing fan.

This way, the pressure losses in ducts were nonexistent. Unfortunately, there was also no additional downforce from the action of ejected air on the spoiler. In that case, downforce increased by 18%.

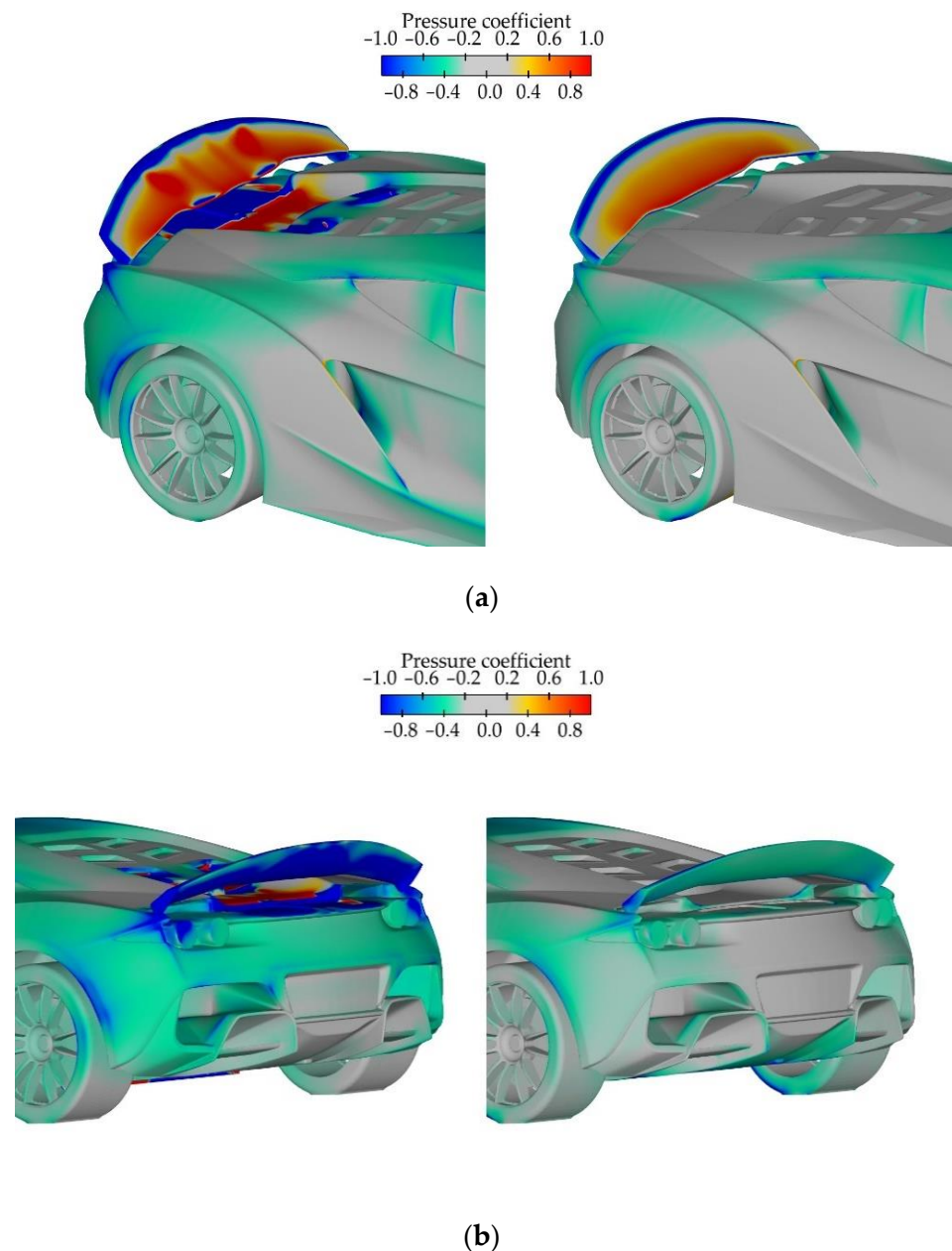


Figure 32. Pressure coefficient for inlet speed of 10 m/s, the case with the FDDG on the left and without FDDG on the right: (a) The upper side of the spoiler; (b) The lower side of the spoiler.

Finally, flow structure changes with increasing car speed are presented with pathlines in Figure 33. It can be seen that, as the car speed increases, the front curtain is blown further and further into the center of the low-pressure chamber. Once the speed exceeds 30 m/s, the side curtains begin to be blown sideways. This is a negative effect and another reason for reducing downforce at increasing speeds. There is potential to achieve better performance if the device is optimized for side curtain stability.

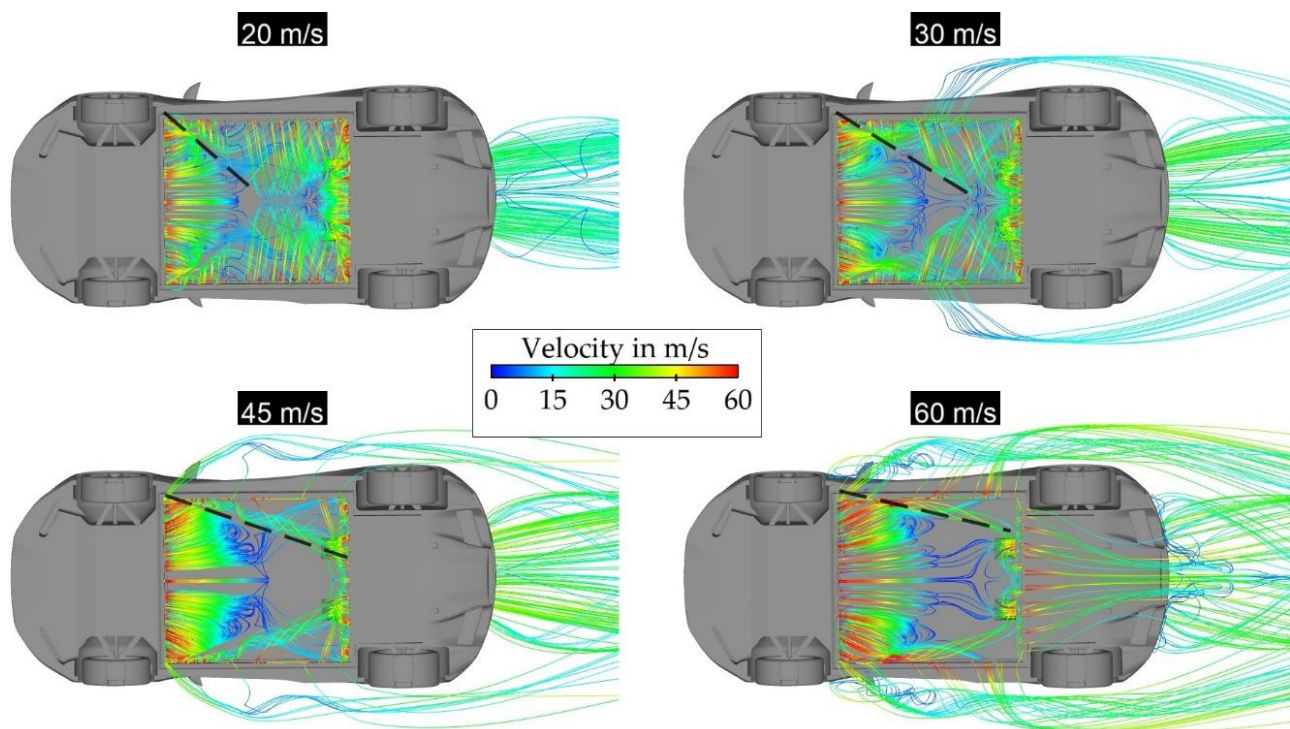


Figure 33. Pathlines released from nozzles for various inlet velocities. The border between pathlines released from the front and side curtains was marked with a dashed line.

3.4. Dynamic Model of a Car with FDDG

Significant changes in sports car construction can be observed recently, and the FDDG fits into the recent trends. Hybrid designs are appearing. In cars, combustion engines and electric motors coexist. In addition to the fuel tanks, there are batteries for electric motors. This means that it is possible to use electric energy quickly, flexibly, and intensively. From the results presented in this paper, it is observed that fan systems lowering pressure under the car are needed only temporarily in certain states of vehicle motion. This is the case during rapid acceleration, rapid braking, and traversing road curves. Fast sports cars are equipped with engines of very high power which, in many driving conditions, cannot be used. At the moment, there are already combinations of combustion engines and electric motors, such as the Koenigsegg Gemera [31].

To show the potential effect of the additional device (FDDG) on the vehicle performance, some simple simulations of the vehicle motion were carried out using its aerodynamic characteristics obtained earlier.

3.4.1. Acceleration

During acceleration, due to traction limitations, only part of the potential power of the engines can be transferred to the contact between the tires and the road. This can be increased by using natural or artificial means to generate additional aerodynamic force pressing the body against the ground. In parallel with the generation of drive force transmitted to the wheels, electrical energy stored in the batteries can be used to activate a fan system that generates additional aerodynamic downforce increasing the transferable traction power. Hypothetical devices can generate about 2000 N of downforce using a not-optimized system of nozzles supplied by the electric fans of total power consumption of about 25 kW, only in short periods, when the car speed is too slow to generate aerodynamic downforce in a conventional way.

A series of simulations based on a simple car dynamics model were performed. To model acceleration the following formula was used:

$$\begin{cases} a = \mu g + \frac{\mu F_z}{m} - F_d & \text{for } v \cdot (\mu F_z + \mu m g + F_d) < P_{limit} \\ a = \frac{P}{v} - 2 \cdot F_d & \text{for } v \cdot (\mu F_z + \mu m g + F_d) > P_{limit} \end{cases} \quad (7)$$

and to simulate braking:

$$a = -\mu g - \frac{\mu F_z}{m} - F_d \quad (8)$$

and maximum cornering radius R was calculated from the equation:

$$R = \frac{mv^2}{\mu - (mg + F_z)} \quad (9)$$

where:

- a —acceleration in m/s^2
- μ —friction coefficient (0.8)
- g —gravitational acceleration in m/s^2
- F_z —downforce in N
- F_d —drag force in N
- m —car mass (1300 kg)
- v —car velocity in m/s
- P —power in W
- P_{limit} —engine power (588,000 W)

In the acceleration calculation, a power limiter was taken into account, coming from the maximum engine power.

In Figure 34, the acceleration characteristics of the car with and without an FDDG are shown. There is much higher acceleration at low speeds due to the downforce generated by the FDDG. When the car reaches a speed where the FDDG stops working, it is turned off and retracted under the car. The increased downforce decreases acceleration time to 100 km/h from 3.6 s to 3.04 s, and to 200 km/h from 7.56 s to 6.89 s. Due to the simplicity of the model, the estimation should be treated as rough, but it shows the huge potential of the proposed device.

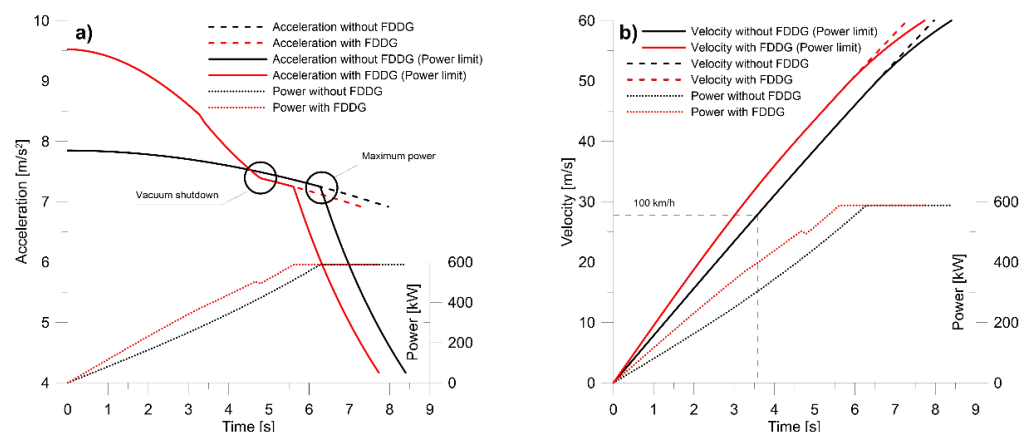


Figure 34. Comparison of car performance equipped with FDDG and without it in acceleration from a full stop: (a) Acceleration; (b) Velocity.

3.4.2. Cornering

When cornering, the limitations of the transmission of lateral forces by the tires mean that there is still an excess of engine power available. In particular, in the case of hybrid drivetrains, this surplus can be effectively used to artificially generate aerodynamic

downforce and thus increase the amount of lateral force transmitted by the tires at the road contact.

In Figure 35, the comparison of possible maximum velocity during cornering dependent on the corner radius and car configuration (with or without FDDG) is presented. The differences are not great. They do not exceed several kilometers per hour. Therefore, it seems that the use of an FDDG would be to extend safety margin, rather than to increase cornering speed. Small changes result from the relatively small value of generated downforce by fans (2000 N) to the mass of the vehicle (1300 kg). Slightly better results could be obtained for the stronger downforce or lighter vehicle. Additional series in Figure 35 shows the effect of the FDDG on cornering radius velocity for a prototype race car weighing 925 kg.

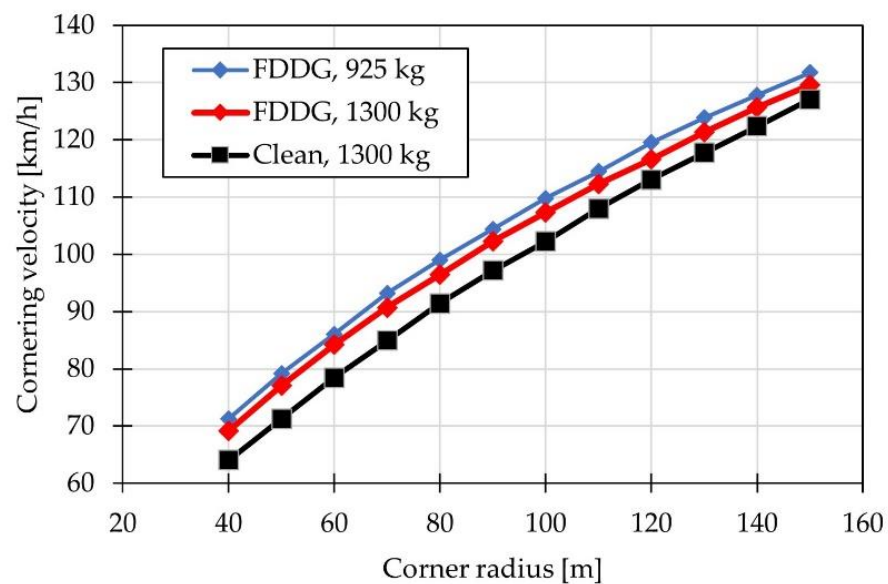


Figure 35. Comparison of maximum velocity during cornering with and without FDDG.

3.4.3. Braking

During braking, its intensity and effectiveness can be increased by a natural or artificial increase in aerodynamic downforce. Temporarily required electrical energy for fans generating additional downforce can be obtained from the electric regenerative braking system or simply from the batteries.

In Figure 36, the braking process characteristics from a set speed of 60 m/s (216 km/h) to a full stop of the vehicle is shown.

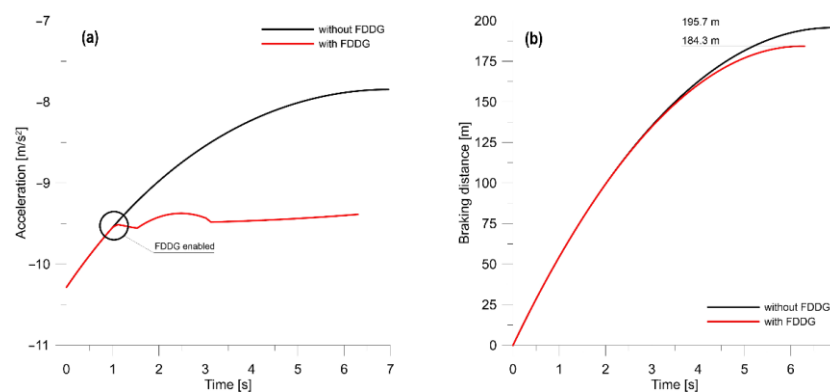


Figure 36. Comparison of car performance equipped with FDDG and without it in braking from a set speed of 216 km/h: (a) Deceleration; (b) Braking distance.

The diagram in Figure 37 shows the differences in the braking distances for different speeds of braking commencement without and with the FDDG device in operation. It can be seen that for lower speeds, the use of the FDDG significantly reduces the braking distance. The higher the speed, the relative benefit from the use of the device decreases; but, for braking from 60 m/s (216 km/h), it still gives a significant reduction in braking distance by 5.8%.

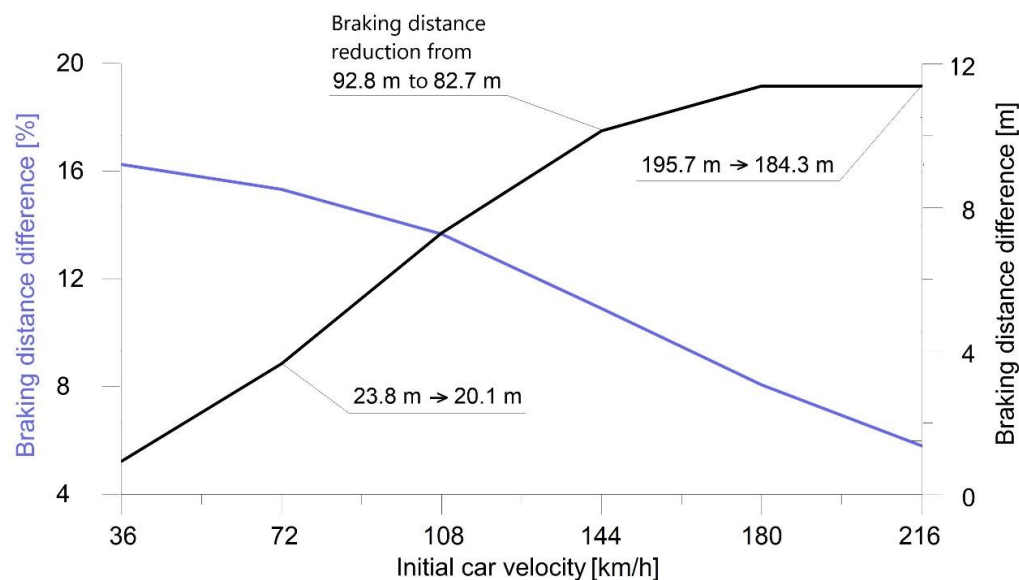


Figure 37. Differences of braking distance in function of speed of braking commencement, with and without FDDG.

It seems that the FDDG working as a system supporting the operation of car brakes would be useful in passenger cars moving with low and average speeds.

4. Conclusions

- The presented solution is the first approximation showing the potential construction possibilities and advantages of the FDDG with air curtains.
- In the tested application of a sports car, the device provided additional downforce, 2600 N at zero velocity: to 1000 N at 40 m/s, using 17 kW of power supplying idealized fans. Koenigsegg Agera R, according to the official data [32], generates 3000 N total downforce at 250 km/h (69.5 m/s).
- Most importantly, the area of effective use of artificially generated aerodynamic downforce can be very wide. In the last subsections of the article, scenarios of fan-enhanced acceleration and braking were studied. The acceleration time to achieve 100 km/h was reduced from 3.6 s to 3.0 s. In the case of braking from 216 km/h to a halt, the braking distance was reduced by 11 m.

Many elements of the device should be optimized: integration of the device with the existing aerodynamic features, placement of outlet ducts, connections between the front and side curtains, etc. Ultimately, the technical implementation of the fans have to be considered. Fan thickness, performance curve, and outlet swirl velocity should also be taken into account. All of this will be the subject of further work.

There are also several limitations of the presented solution. The use of curtains generating air streams with high velocity directed towards the ground in case of its contamination with sand, dust, and water will generate their lift and dispersion around the car body (see Figure 33). There are pictures of a Chaparral 2J vehicle generating a stream of dusty air behind a fast-moving body.

Whether the advantages or disadvantages of the solution will prevail is difficult to predict at this time. The feedback from drivers who have driven the Chaparral 2J has

been and remains enthusiastic. Feedback from drivers left behind is less enthusiastic, but everyone appreciates the clear path ahead.

Author Contributions: Conceptualization, J.P.; methodology, J.P.; software, J.P., M.S. and A.P.; validation, J.P., M.S. and A.P.; formal analysis, J.P., M.S. and A.P.; investigation, J.P., M.S. and A.P.; resources, J.P., M.S. and A.P.; data curation, J.P. and M.S.; writing—original draft preparation, J.P., M.S. and A.P.; writing—review and editing, J.P., M.S. and A.P.; visualization, J.P., M.S. and A.P.; supervision, J.P.; project administration, J.P. All authors have read and agreed to the published version of the manuscript.

Funding: This research received no external funding.

Institutional Review Board Statement: Not applicable.

Informed Consent Statement: Not applicable.

Data Availability Statement: Not applicable.

Acknowledgments: The authors thank Arrinera SA for allowing the geometry of the Hussarya vehicle to be used to perform the aerodynamic analyses presented in this paper.

Conflicts of Interest: The authors declare no conflict of interest.

References

1. Katz, J.; Garcia, D. Aerodynamic effects of Indy car components. *SAE Tran.* **2002**, *111*, 2322–2330.
2. Mezger, H. Der Porsche 4,5-l-Rennsportwagen Typ 917, Teil 2, ATZ, BD.; 1969; Volume 71, pp. 417–423. Available online: <https://presskit.porsche.de/museum/en/2019/topic/anniversaries/porsche-celebrates-50-years-of-the-917/hans-mezger-the-porsche-917-chief-engineer.html> (accessed on 15 September 2021).
3. Lamar, P. Aerodynamics & The Group Seven Racing Car. In Proceedings of the AIAA Symposium on The Aerodynamics of Sports & Competition Automobiles, Los Angeles, CA, USA, 20 April 1968.
4. Hucho, W.-H. (Ed.) *Aerodynamics of Road Vehicles*, 4th ed.; SAE International: Warrendale, PA, USA; Materials Park, OH, USA, 1998; p. 918. [CrossRef]
5. Savkoor, A.R.; Chou, C.T. Application of Aerodynamic Actuators to Improve Vehicle Handling. *Veh. Syst. Dyn. Int. J. Veh. Mech. Mobil.* **1999**, *32*, 345–374.
6. Kataoka, T.; China, H.; Nakagawa, K.; Yanagimoto, K.; Yoshida, M. Numerical simulation of road vehicle aerodynamics and effect of aerodynamic devices. *SAE Trans.* **1991**, *100*, 722–734.
7. Winkelmann, H. Aerodynamics of the new BMW Z4. In Proceedings of the 4th MIRA International Vehicle Aerodynamics Conference, Gaydon, UK, 25–26 October 2006.
8. Hall, J.E.; Mrlik, J.R.; Musser, J.G.; Winchell, F.J. Aerodynamic Spoiler for Automotive Vehicles. US Patent 3455594, 15 July 1969.
9. Ludwig, K.; Bruder, W.A. Aerodynamic Braking Mechanism for Motor Vehicles. U.S. Patent 2932370A, 11 June 1956.
10. Broniszewski, J.; Piechna, J. A fully coupled analysis of unsteady aerodynamics impact on vehicle dynamics during braking. *Eng. Appl. Comput. Fluid Mech.* **2019**, *13*, 623–641. [CrossRef]
11. Broniszewski, J.; Piechna, J.R. Fluid-Structure Interaction Analysis of a Competitive Car during Brake-in-Turn Manoeuvre. *Energies* **2022**, *15*, 2917. [CrossRef]
12. Kurec, K.; Remer, M.; Mayer, T.; Tudruj, S.; Piechna, J. Flow control for a car-mounted rear wing. *Int. J. Mech. Sci.* **2019**, *152*, 384–399. [CrossRef]
13. Piechna, J.R.; Kurec, K.; Broniszewski, J.; Remer, M.; Piechna, A.; Kamieniecki, K.; Bibik, P. Influence of the Car Movable Aerodynamic Elements on Fast Road Car Cornering. *Energies* **2022**, *15*, 689. [CrossRef]
14. Szudarek, M.; Piechna, J. CFD Analysis of the Influence of the Front Wing Setup on a Time Attack Sports Car’s Aerodynamics. *Energies* **2021**, *14*, 7907. [CrossRef]
15. Rong, B.Z. Jim Hall and the Chaparral 2J: The Story of America’s Most Extreme Race Car. Available online: <https://www.roadandtrack.com/motorsports/a32350/jim-hall-chaparral-2j-history/> (accessed on 28 June 2022).
16. Falconer, R.; Nye, D. *Chaparral*; Motorbooks International: Osceola, WI, USA, 1992.
17. O’Callaghan, D. Chaparral 2J: Here’s How It Worked and What Happened When It Raced. Available online: <https://www.hotcars.com/chaparral-2j-see-how-it-worked-and-what-happened-when-it-raced/> (accessed on 28 June 2022).
18. This Was the Brabham BT46B, the Revolutionary Fan Car That Formula 1 Had to Ban for Bullying. Available online: <https://tekdeeps.com/this-was-the-brabham-bt46b-the-revolutionary-fan-car-that-formula-1-had-to-ban-for-bullying/> (accessed on 28 June 2022).
19. Secrets of the Lotus 79 Skirts. Available online: <https://classicteamlotus.co.uk/en/news/posts/2021/secrets-of-the-lotus-79-skirts/> (accessed on 28 June 2022).
20. Dernie, F.W. Vehicle Suspension Systems. U.S. Patent 4861066, 29 August 1989.

21. Active Suspension. Available online: <https://www.motorsportmagazine.com/archive/article/december-2001/69/active-suspension> (accessed on 28 June 2022).
22. Suspension III: Active Suspension Systems. Available online: <https://www.edmunds.com/car-technology/suspension-iii-active-suspension-systems.html> (accessed on 28 June 2022).
23. Is the Aston Martin DB11's Virtual Spoiler a Gimmick? Available online: <https://www.carthrottle.com/post/wpm4dxr/> (accessed on 28 June 2022).
24. Ehrich, F.F. The Curtain Jet. *J. Aerosp. Sci.* **1961**, *28*, 855–860. [[CrossRef](#)]
25. Strand, T. Inviscid incompressible flow theory of static peripheral jets in proximity to the ground. *J. Aer./Space Sci.* **1961**, *28*, 27–33. [[CrossRef](#)]
26. Roche, J.T.D. The peripheral jet theory. In *Applied Mechanics*; Görtler, H., Ed.; Springer: Berlin/Heidelberg, Germany, 1966. [[CrossRef](#)]
27. Makowski, F.T.; Kim, S.E. *Advances in External-Aero Simulation of Ground Vehicles Using the Steady RANS Equations*; Technical Paper; SAE: Warrendale, PA, USA, 2000; No. 2000-01-0484. [[CrossRef](#)]
28. Shih, T.H.; Liou, W.; Shabbir, A.; Yang, Z.; Zhu, J. A new k- ϵ eddy viscosity model for high reynolds number turbulent flows. *Comput. Fluids* **1995**, *24*, 227–238. [[CrossRef](#)]
29. Menter, F.R. Two-Equation Eddy-Viscosity Turbulence Models for Engineering Applications. *AIAA J.* **1994**, *32*, 1598–1605. [[CrossRef](#)]
30. Cooke, G.C.; Duffy, R.E. Forward-Speed Effects on Peripheral-Jet Ground Support Systems. *J. Aircr.* **1972**, *9*, 675–681. [[CrossRef](#)]
31. Koenigsegg Gemera. Available online: <https://www.koenigsegg.com/model/gemera> (accessed on 28 June 2022).
32. Koenigsegg Agera, R. Available online: <https://www.koenigsegg.com/technical-specifications-agera-r> (accessed on 28 June 2022).